TIME DOMAIN REFLECTOMETRY (TDR) TECHNIQUES FOR THE DESIGN OF DISTRIBUTED SENSORS

by

Jeffrey Allen Stastny

Thesis submitted to the Faculty of the

Virginia Polytechnic Institute and State University

in partial fulfillment of the requirements for the degree of

MASTER OF SCIENCE

in

Mechanical Engineering

APPROVED:

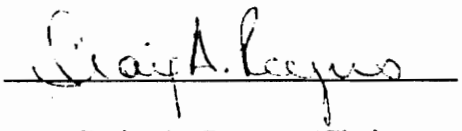

Dr. Craig A. Rogers, Chairman

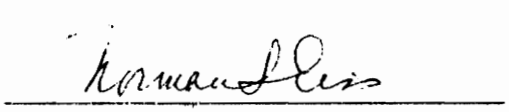

Dr. Norman S. Eiss

Dr. Curtis H. Stern

October, 1992

Blacksburg, Virginia

Time Domain Reflectometry (TDR) Techniques for the Design of Distributed Sensors

by

Jeffrey Allen Stastny

Committee Chairman: Dr. Craig A. Rogers

Mechanical Engineering

Abstract

Parametric design models were created to optimize cable sensitivities in a structural health-monitoring system. Experiments were also conducted to determine the sensitivity of a working system. The system consists of time domain reflectometry (TDR) signal processing equipment and specially designed sensing cables. The TDR equipment sends a high-frequency electric pulse (in the gigahertz range) along the sensing cable. Any change in electric impedance along the cable reflects some portion of the electric pulse back to the TDR equipment. The time delay, amplitude, and shape of the reflected pulse provides the means to respectively locate, determine the magnitude, and indicate the nature of the change in impedance. The change in the sensing cable impedance may be caused by cable elongation (change in resistance), shear deformation (change in capacitance), corrosion of the cable or the materials around the cable (change in inductance), etc.

The sensing cables are an essential part of the health-monitoring system because the cable

design parameters determine the cable impedance sensitivity to structural changes. By using parametric design models, the optimum cable parameters can be determined for specific cases and used to select or design an appropriate cable. Proof-of-concept and resolution experiments were also conducted to provide, respectively, verification and sensitivity of the system.

Acknowledgements

An enormous amount of thanks is deserved by the many people who have helped me achieve this thesis. My advisor, Dr. Craig Rogers, is greatly appreciated for the financial support and the mental guidance/enlightenment that he has bestowed upon me. The people at CIMSS have always been there for help in any way, shape, or form. Their support will never be forgotten. The comments and ideas of my other committee members, Dr. Norm Eiss and Dr. Curtis Stern, were essential in completing this project. Most of all, my family deserves thanks for supporting me on my exodus from Oregon. Without the examples of determination and hard work they have provided for me, I would not have believed this project to be possible. They have always been there to get me started when I began to falter. Thank you for the greatest "bat" of all, the love of a family. Finally, I would like this thesis to commemorate my grandmother, Mariam Stastny. It was her patient teaching manner that started my enjoyment of math, the subject which put me on the path to an engineering career.

Table of Contents

List of Figures

List of Tables

Nomenclature[1,2]

Δl	Incremental distance, meters
Δl_n	Incremental length at nth point, meters
ΔW	Incremental work, joules
ϵ	Permittivity, farads/meter
ϵ_0	Dielectric constant or permittivity of a vacuum, farads/meter
ϵ_l	Linear strain
μ	Permeability, henrys/meter
υ_c	Poisson's ratio for the conductors
ρ	Cylindrical radius, meters
ρ	Reflection coefficient
ρ_c	Conductor resistivity, ohm-meter
ρ_l	Charge density of a line charge, coulombs/meter
σ	Conductivity, siemens/meter
$\phi(x, y, z)$	Absolute potential at a point, volts
ϕ_{ab}	Potential difference between radius a and b, volts

[1]Vector quantities are indicated by **bold** face in the text.

[2]Vector quantities are indicated by overline arrows in the equations and illustrations.

ϕ_{fi}	Potential difference between points P_f and P_i, volts
ϕ_f, ϕ_i	Absolute potential at points P_f and P_i, volts
ϕ_m	Magnetic scalar potential, amperes
ω	Angular velocity, radians/second
A	Cross-sectional area of conductors, meters^2
a,b	Radial dimensions, meters
$\boldsymbol{a}_l$	Direction vector along conductor length
$\boldsymbol{a}_x$, $\boldsymbol{a}_y$, $\boldsymbol{a}_z$	Rectangular direction vectors
$\boldsymbol{a}_\rho$, $\boldsymbol{a}_\phi$, $\boldsymbol{a}_z$	Cylindrical direction vectors
$\boldsymbol{a}_r$, $\boldsymbol{a}_\theta$, $\boldsymbol{a}_\rho$	Spherical direction vectors
$\boldsymbol{B}$	Magnetic flux density, webers/meter^2 = tesla
C	Capacitance per unit length, farads/meter
c_1, c_2	Paths c_1 and c_2
$\boldsymbol{D}$	Electric flux density, coulombs/meter^2
D	Distance between X and wave source, meters
d, D, D_0	Coaxial cable dimensions, meters
d	Charge center dimension, meters
$d\boldsymbol{l}$	Differential length vector, meters
$\boldsymbol{E}$	Electric field, volts/meter
e	Radial dimension at property change, meters
E_n	Electric field intensity at nth point, volts/meter
E_r, E_i	Alternate notation for reflected and incident voltage, volts

F	Force between charges, newtons
F_{ext}	External scalar force, newtons
G	Conductance per unit length, siemens/meter
H	Magnetic field intensity, amperes/meter
i	Imaginary number
I_{in}, I_X	Current into the system and at X, amperes
J	Conduction current density, amperes/meter^2
K	Constant in potential derivation
L	Inductance per unit length, henrys/meter
L_{ext}	External inductance, henrys/meter
P_i, P_f	Initial and final points along conductor
Q	Total charge, coulombs
Q_1, Q_2	Point charges at points 1 and 2, coulombs
R	Resistance per unit length, ohms/meter
R	Distance between points 1 and 2, meters
R	Radius from charge to a reference point, meters
r	Radius from charge to a point, meters
r_0	Radius constant for equipotential cylinders, meters
R_1, R_2	Reference radii, meters
r_1, r_2	Radial components in spherical coordinates, meters
s	A closed surface
T	Transit time, seconds

T_r	Pulse rise time, seconds
V_0	Voltage potential, volts
V_c	Velocity of light, meters/second
V_{in}, V_X	Voltage into the system and at X, volts
V_p	Velocity of propagation, meters/second
V_r, V_i	Reflected and incident voltage, volts
W	Total work required to move a charge, joules
w, W	Parallel cable dimensions, meters
X	A point along a sensor cable
x, y, z	Rectangular coordinates, meters
x_0	Axis location constant for equipotential cylinders, meters
Z_0, Z_X	Characteristic impedance and impedance at X, ohms
Z_L	Impedance load on transmission line, ohms

The first step binds one to the second.

- French Proverb

Chapter 1

Introduction

From bridges to skyscrapers, and airplanes to trains, today's deteriorating civil infrastructure and public transportation vehicles are a national crisis. Examples of structural failure can be found from the past (the S. S. Schenectady (1943), a U. S. T2 tanker that buckled) to the present (Schoharie Creek Thruway Bridge collapse, 1987). Not all occurrences are from normal wear and tear, but even those due to natural disasters, such as floods and earthquakes (Bay Bridge and Nimitz Freeway during the Loma Prieta earthquake in 1989 (Castro, 1989)), could have benefitted from a damage detection system to warn of imminent failure. On April 23, 1988, this need for a damage detection system in public works and vehicles was abruptly brought to the world's attention by the fatigue failure of an Aloha Airlines Boeing 737 (O'Lone, 1988). The call for these systems has already been placed by the aircraft industry (Gerardi, 1990) and by public works (Chong, Scalzi, and Dillon, 1990).

A health-monitoring system would act as the "nerves" for a structure, similar to a biological nervous system. It should be able to determine the location, type, and extent

of damage. An ideal configuration, as stated by Amoto (1992), will function such that "when the structure is hurt, it will in effect feel pain and let someone know". This proposed system could be used to determine where repairs need to be made and/or if the structures are even safe for use.

Several types of systems have been proposed using fiber optics (Measures, 1989), piezoelectrics (Crawley and de Luis, 1987), and shape memory alloys (Ikegami et al., 1990) as the active sensor. Rogers, Liang, and Li (1991) have even suggested a method of active damage control (ADC) to reduce crack damage in composites. The problem with these systems is that true "distributed" sensing is not being used. A distributed system (see Figure 1.1a) will give damage information at any point along the length of the structure. The previously mentioned systems rely on a series of discrete sensors or sensors mounted at specific points within a structure to get quasi-distributed sensing (see Figure 1.1b). Even the fiber optic systems which are considered to have good resolution rely on fiber splices placed at specific points to determine the location of damage. The resolution or distance between sensing points, therefore, relies on how closely the sensors can be placed without adversely affecting the structure. Time domain reflectometry (TDR) is one method which provides true distributed sensing capability.

TDR is best described as "closed-loop radar" (Hewlett-Packard, 1964), where information is derived from the reflections of a voltage pulse sent through a transmission system (a cable). The resolution of this technique is limited by the sensitivity of the TDR

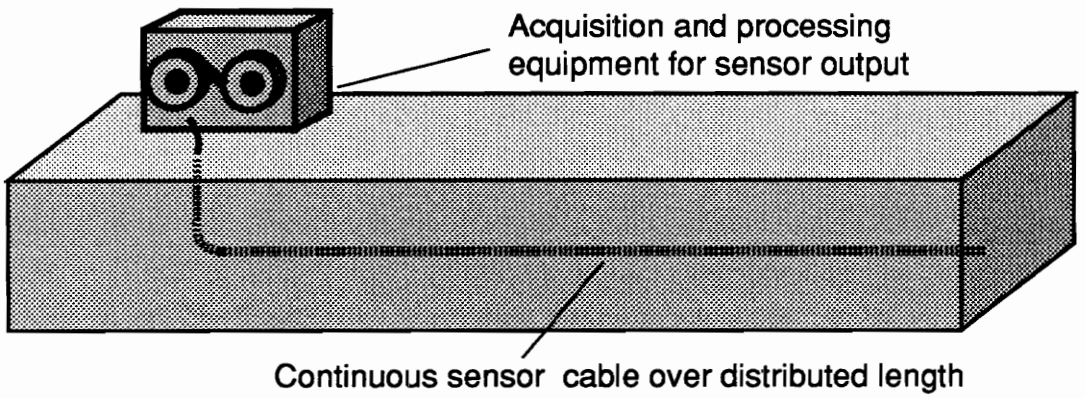

(a)

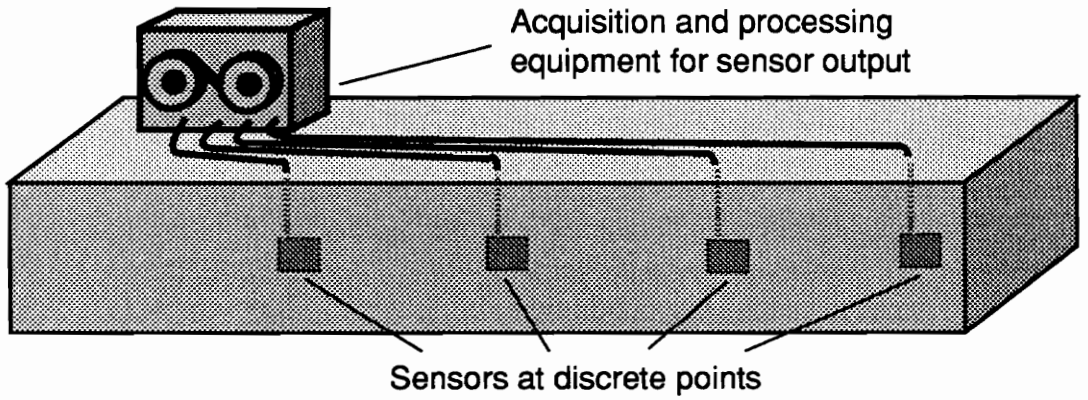

(b)

Figure 1.1 Comparison of (a) distributed sensing with continuous sensors and (b) quasi-distributed sensing with discrete sensors.

equipment, but it can be enhanced by carefully designed cables. This type of system has the advantage of being proven effective in other areas of research. Key examples are composite structures with optical fibers (Jackson, 1984), mining wall maintenance (Panek and Tesh, 1981), shock and detonation wave monitoring (Dick and Parrish, 1986), and ionic conductivity and permittivity measurements (Dorenbos and den Hartog, 1988).

TDR is very useful in revealing information about impedance discontinuities in a cable. A discontinuity occurs when the cable impedance properties are different from those in a previous cable section. When a discontinuity is encountered, a portion of the incident pulse is reflected back with the magnitude and shape of the reflected pulse depending on the type of discontinuity. The time lag of the reflected signal can be used to determine the near real-time location of the discontinuity if the pulse propagation velocity is known for the cable. By relating the cable discontinuity to the structural property change which creates it, the TDR data can be used to determine the location, type, and magnitude of the damage in the structure. In combination, this information provides a clear "sensation" of the damage sites within the structure and can help determine what procedures are needed to repair the damage. This thesis considers the use of these methods to develop a structural, health-monitoring, sensing system.

Chapter one covers an introduction to TDR methods and the motivation for this research. The various other projects in this area are also covered in a review of current literature.

Chapter two is used to develop the electromagnetic theory for the various sensor types. The derivation begins with Coulomb's Law and continues through the relationships for electrical impedance related to stresses or strains within the host structure. These are pursued for coaxial and two-wire sensing cables. The basis for the parametric studies is also laid out.

Chapter three discuss the analysis of possible sensors through the use of parametric studies. The specific equations used are produced. Sample case study results are given to show design optimization possibilities for the derived models.

Chapter four is used to discuss the experimental set-up for the model verification. The test results are given for specific case studies. The validity of the model is determined by a comparison between the theoretical results and the experimental results.

Chapter five summarizes the project by stating the conclusions and recommendations of this research. Finally, goals and applications of this project are proposed for future researchers.

1.1 Introduction to TDR

Fatigue, fracture, and damage, as discussed previously, are a large concern in the modern day of composite materials. Composites, as defined in Jones (1975), combine

two or more materials on a macroscopic scale to form a useful material. They could include any mixture of materials used to construct a structure from concrete to graphite/epoxy laminates. Recently, mechanisms have been proposed to control damage in composite material systems. As stated before, one example is active damage control (Rogers, Liang, and Li, 1991). To be effective, new control systems must be able to sense where, what type of, and how much damage is occurring in a structure. A distributed sensing mechanism similar to a biological nervous system must be developed to meet this requirement. This research work is involved in developing such mechanisms through the use of time domain reflectometry (TDR) techniques.

The basics of these techniques were derived by L. R. Moffitt in his 1964 article "Time Domain Reflectometry - Theory and Applications" (Moffitt, 1964). He initially used TDR to locate and evaluate discontinuities in coaxial power transmission cables (the primary use of the method to this day). A typical system (see Figure 1.2) employs a transmission medium (transmission or sensor cable), a step generator, and an oscilloscope. A voltage step is propagated down the transmission line under investigation. Some of the electric step pulse is reflected back when electric impedance discontinuities are encountered. The reflected step signal reveals the characteristic impedance of the transmission line and shows both the position and the nature (resistive, inductive, or capacitive) of each discontinuity along the line. All of the information (position, nature, and extent of the discontinuities) is immediately available from the oscilloscope display.

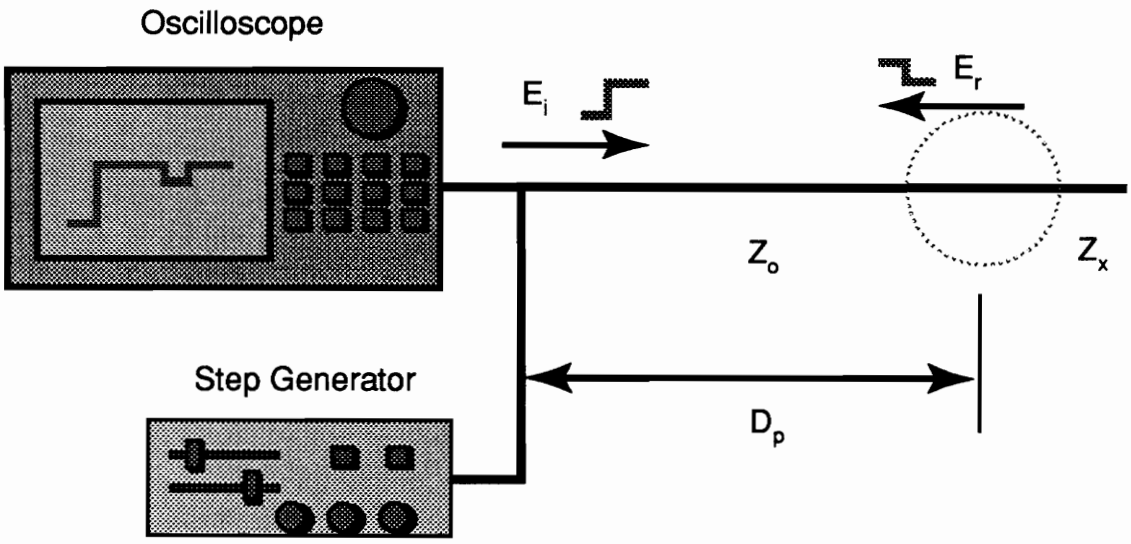

Figure 1.2 Typical TDR system.

Figure 1.3 shows the classical model for transmission lines. The model assumes a continuous structure with electrical properties of resistance, R, inductance, L, capacitance, C, and conductance, G, with $\omega = 2\pi f$ where f is the frequency of the pulse. If the line is infinitely long, and R, L, C, and G are defined per unit length, the characteristic impedance of the line, Z_0 , is calculated as

$$Z_0 = \sqrt{\frac{R + i\omega L}{G + i\omega C}} \quad , \tag{1.1}$$

where G is usually very small (inverse of the dielectric resistance).

The voltage, E, and current, I, are related at any point by the characteristic impedance, Z_0, of the line:

$$Z_0 = \frac{E_x}{I_x} = \frac{E_{in}}{I_{in}} \quad . \tag{1.2}$$

A voltage pulse introduced at the generator requires a finite time to travel to a point X as shown in Figure 1.2. If the electric impedance at point X changes due to extrinsic reasons, the mismatch between Z_0 and Z_x results in the propagation of a second wave up the line towards the source. The reflected wave is the energy that cannot be delivered over the point X. The degree of the discontinuities in the electric impedances, Z_0 and Z_x, is indicated by the ratio of the reflected wave to the incident wave which originated from the source. This ratio is called the reflection coefficient, ρ , and is related to the line impedance by:

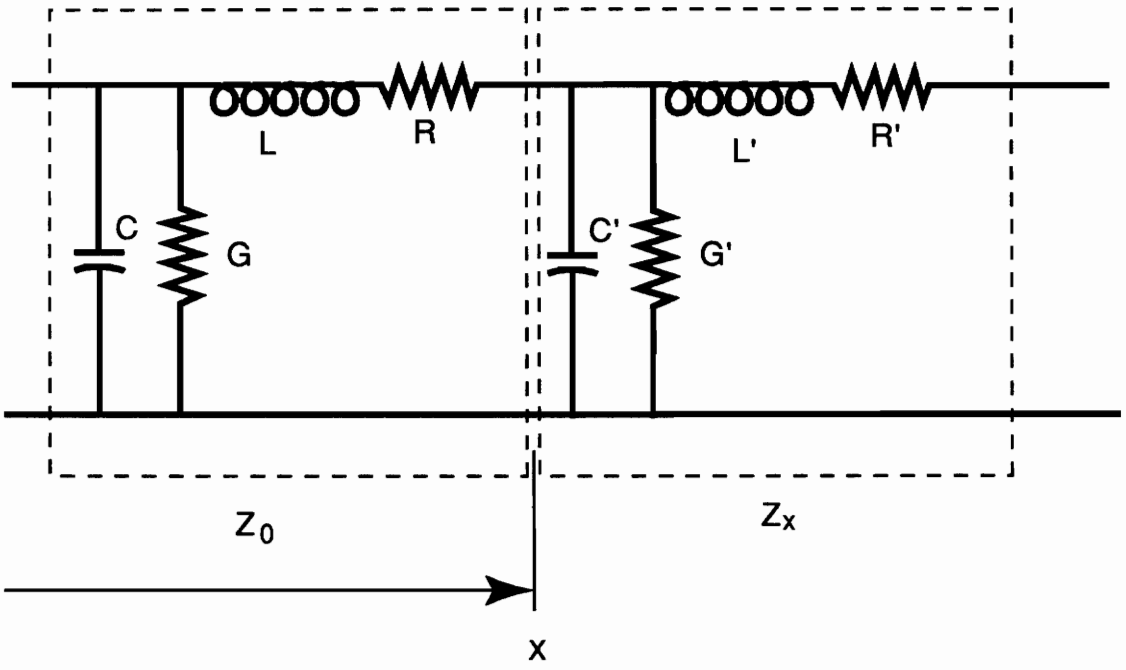

Figure 1.3 Classical transmission line model.

$$\rho = \frac{E_r}{E_i} = \frac{Z_x - Z_0}{Z_x + Z_0} \quad , \tag{1.3}$$

where E_r is the reflected voltage and E_i is the incident voltage.

The reflected wave is readily identified since it is separated in time from the incident wave. This time delay is used to determine the location of the mismatching impedance. The distance between the mismatching point and the wave source (the generator), D_p, can be expressed as:

$$D_p = V_p \frac{T}{2} \quad , \tag{1.4}$$

where T is the transit time from the monitoring point to the mismatch and back again, as measured on the oscilloscope (Figure 1.2). The wave propagation velocity, V_p, of a transmission line can be pre-determined from the relative dielectric constant, ϵ_r, of the transmission line insulaton to be

$$V_p = \frac{V_c}{\sqrt{\epsilon_r}} \quad , \tag{1.5}$$

where V_c is the velocity of light.

The reflected voltage wave appears on the oscilloscope display algebraically added to the incident wave as shown in Figure 1.2. The shape of the reflected wave is also valuable since it reveals both the nature and magnitude of the mismatching impedance. Figure 1.4 shows some of the typical TDR wave shapes and the corresponding resistive

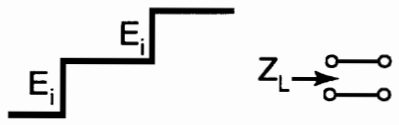

(a) Open circuit termination ($Z_L = \infty$)

(a) $E_r = E_i$ Therefore $\frac{Z_L - Z_o}{Z_L + Z_o} = +1$

which is true as $Z_L \rightarrow \infty$

$\therefore$ Z = open circuit

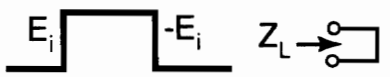

(b) Short circuit termination ($Z_L = 0$)

(b) $E_r = -E_i$ Therefore $\frac{Z_L - Z_o}{Z_L + Z_o} = -1$

which is only true (for finite Z_o) when $Z_L = 0$

$\therefore$ Z = short circuit

(c) Line terminated in $Z_L = 2Z_o$

(c) $E_r = +\frac{1}{3}E_i$ Therefore $\frac{Z_L - Z_o}{Z_L + Z_o} = +\frac{1}{3}E_i$

and $Z_L = 2Z_o$

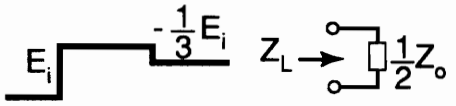

(d) Line terminated in $Z_L = \frac{1}{2}Z_o$

(d) $E_r = -\frac{1}{3}E_i$ Therefore $\frac{Z_L - Z_o}{Z_L + Z_o} = -\frac{1}{3}E_i$

and $Z_L = \frac{1}{2}Z_o$

Figure 1.4 Typical TDR displays and corresponding resistive impedance mismatches (Hewlett-Packard, 1987).

impedance mismatches for an impedance load (Z_L) on the transmission line. If the reflection is caused by inductive or capacitive impedance mismatch (complex impedance), the reflected wave has a certain characteristic shape related to the types of impedance mismatches, as shown in Figure 1.5.

One of the advantages of TDR over other techniques is its ability to handle multiple impedance mismatches or discontinuities. The display for this situation would be similar to Figure 1.6. The two mismatches produce reflections that can be analyzed separately. At the first mismatch, a reflected wave, E_{r1}, is generated where:

$$E_{rl} = \rho_1 E_i = \left[\frac{Z_0'-Z_0}{Z_0'+Z_0}\right] E_i \quad . \tag{1.6}$$

The mismatch at the load also creates a reflection due to its reflection coefficient:

$$\rho_2 = \frac{Z_L-Z_0'}{Z_L+Z_0'} \quad . \tag{1.7}$$

The voltage step incident on Z_L is:

$$(1+\rho_1)E_i \quad , \tag{1.8}$$

and the reflection from the load is:

$$\left[\rho_2(1+\rho_1)E_i\right] = E_{rL} \quad . \tag{1.9}$$

Due to re-reflection at the impedance junction the wave that returns to the monitoring point is:

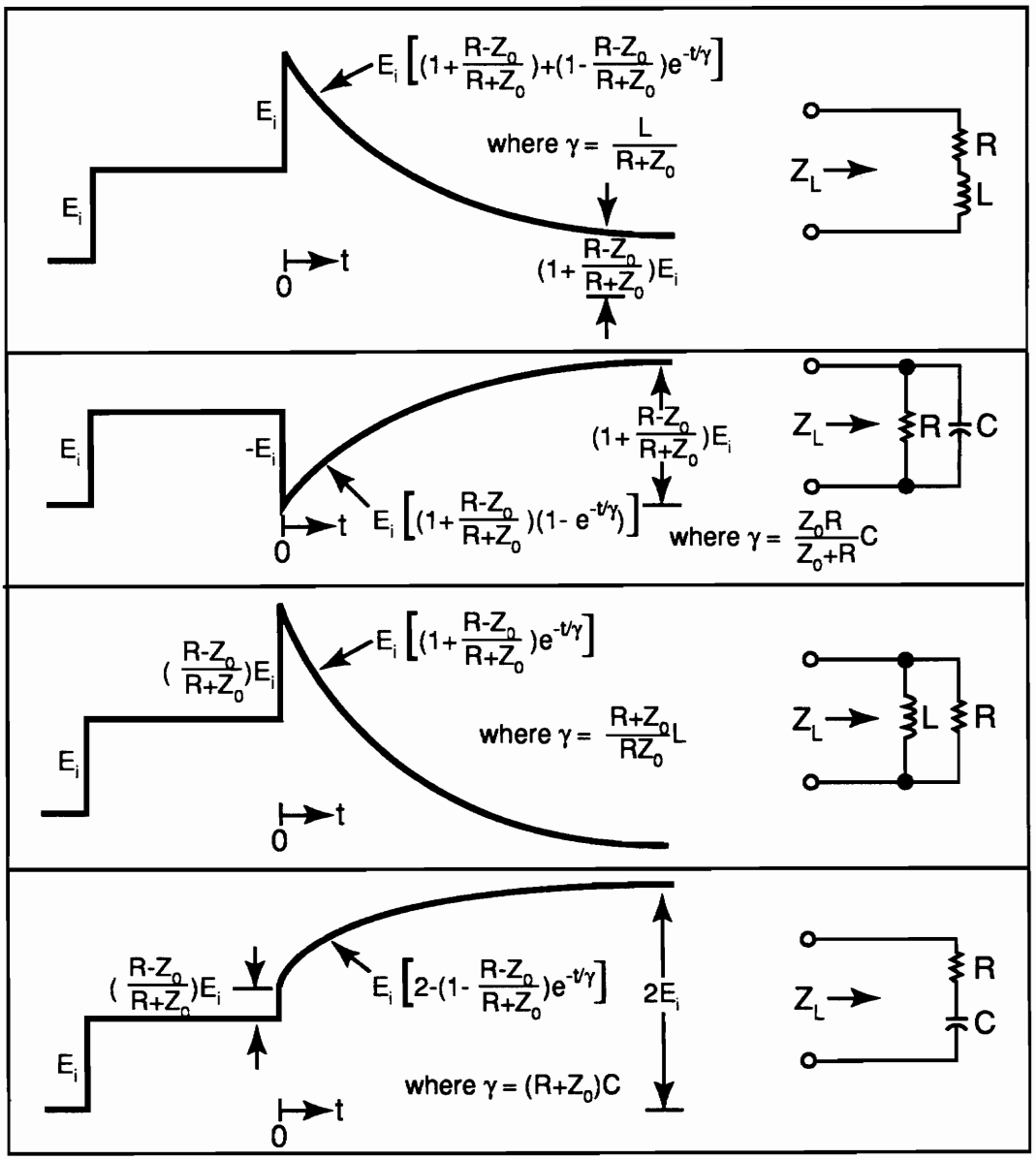

Figure 1.5 Complex impedance mismatches (Hewlett-Packard, 1987).

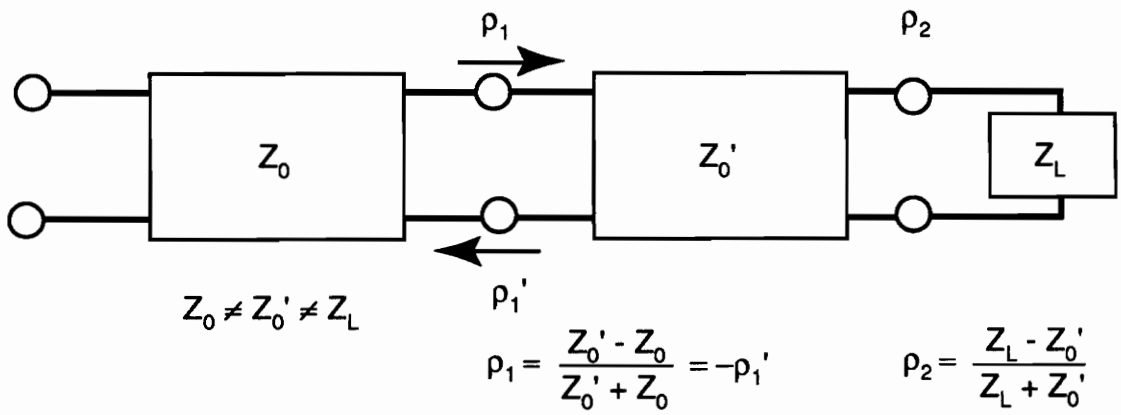

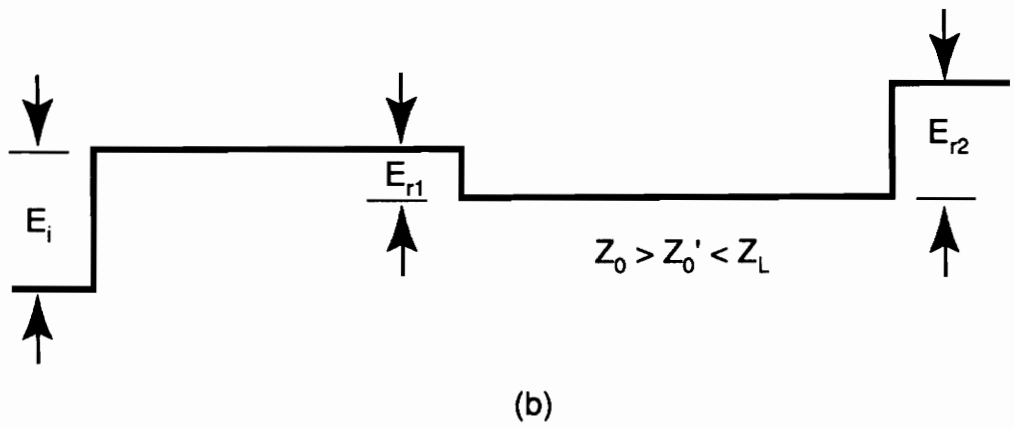

Figure 1.6 Multiple discontinuity (a) circuit diagram and (b) TDR display (Hewlett-Packard, 1987).

$$E_{r2} = (1+\rho_1')E_{rL} = (1+\rho_1')\left[\rho_2(1+\rho_1)E_1\right] \quad . \tag{1.10}$$

Since $\rho_1' = -\rho_1$, E_{r2} may be also be written as:

$$E_{r2} = \left[\rho_2(1-\rho_1^2)\right]E_1 \quad . \tag{1.11}$$

It is now seen that although TDR is useful when observing multiple discontinuities, one must be aware of the slight complications these discontinuities introduce when analyzing the display. The reflection from the first of any number of discontinuities is unaffected by the presence of others; therefore, if it is analyzed first and then corrected, the second discontinuity can be analyzed without the complications introduced by re-reflections.

Two more complications, the step pulse rise time and impedance of the TDR equipment, limit the minimum distance between points and scope of the measurements. The previous analysis was based on a near-zero rise time for the applied step pulse. The rise time for the equipment used was around 45 pico seconds which limits the distance or time resolution of the system. The effect of the finite rise time is to low-pass filter the ideal (zero rise time) response of a given discontinuity. The distance to a discontinuity is given in Equation 4 and can be used to determine the distance between two discontinuities as:

$$\Delta D = \frac{V_c}{\sqrt{\epsilon_r}} \frac{T_2-T_1}{2} \quad , \tag{1.12}$$

where T_2 and T_1 are the two-way travel times. The two discontinuities become indistinguishable when separated by a time (T_2 - T_1) of less than half the system rise time. Therefore, the minimum distinguishable distance between two discontinuities is given by:

$$D_{\min} = \frac{V_c}{\sqrt{\epsilon_r}} \frac{T_r}{4} \quad . \tag{1.13}$$

The minimum distance can be improved by using greater cable dielectric constants or decreasing the equipment rise time. The equipment must also be impedance matched to the transmission line. As shown for two discontinuities, if large changes take place the incident pulse can be dramatically reduced making the size of the reflected signal harder to discern. If the impedance of the sensing equipment is matched to that of the transmission line, the pulse will flow through with few losses. The signal can also be enhanced by increasing the size of the incident pulse, but the rise time may also increase. For these reasons the selection of TDR equipment and transmission mediums is important for obtaining the best signals.

The signals given by TDR analysis are related to the structure within which the sensor is embedded. A unique signal is sent by the sensor under normal conditions (Figure 1.7a). This signal can be normalized to simplify the recognition of changes. Two typical signals are then generated under strain conditions. The first is associated with axial strain and is composed of a resistive step due to symmetrical geometry changes (Figure 1.7b). The second is associated with shear strain and is composed of a

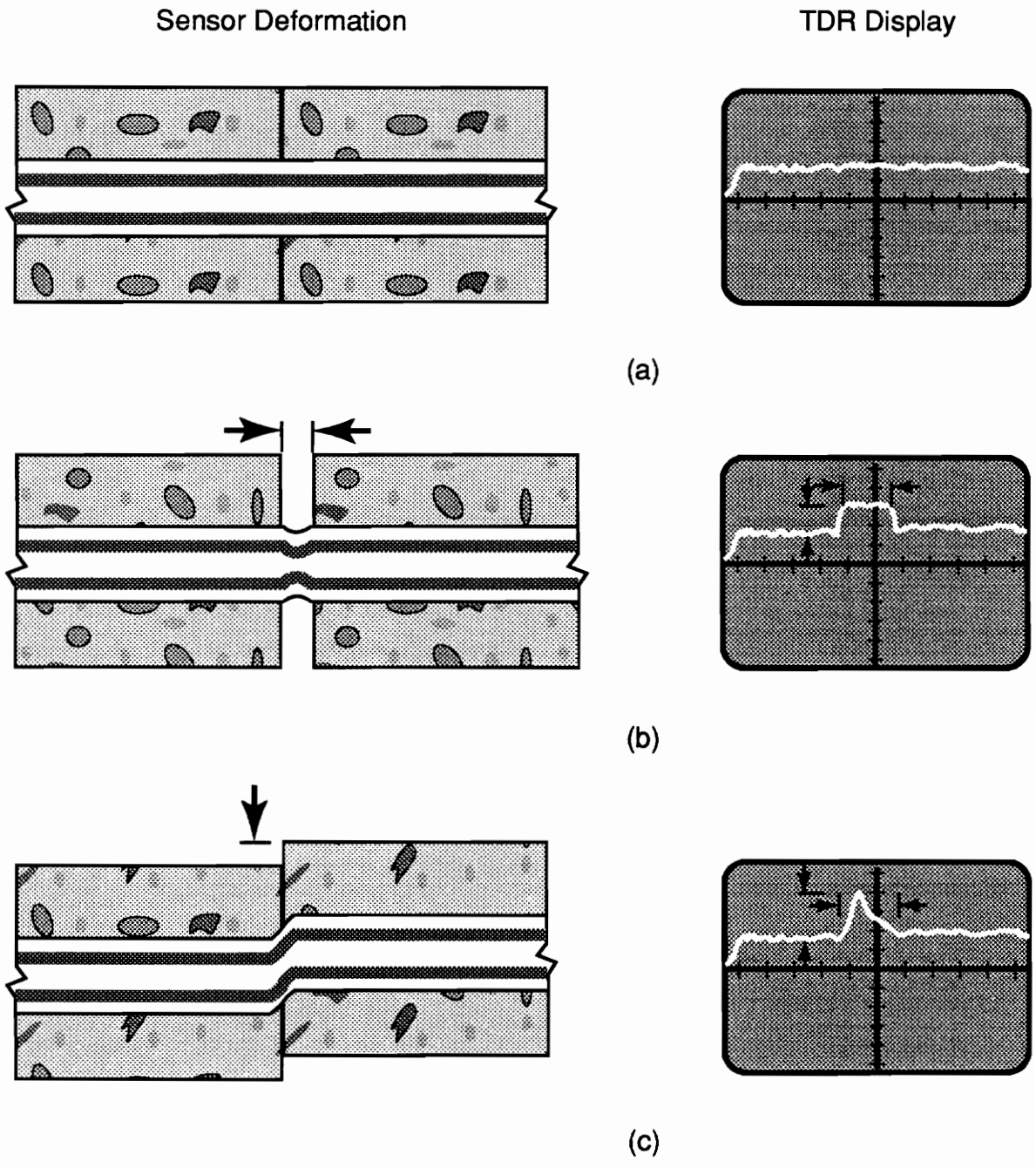

Figure 1.7 Sensor displacement and TDR output for (a) normal conditions (b) axial strain and (c) shear strain.

capacitive spike due to unsymmetrical geometry changes (Figure 1.7c). As shown in Figures 1.7b and 1.7c, the respective TDR output is a step increase and a spike increase for the displayed sensor signal. A normalized display, obtained by subtracting the original unstrain plot from the plot given during strain application, would indicate the specific change that took place (the resistive step in Figure 1.7b or the capacitive spike in Figure 1.7c). Once these responses are catalogued to the host structure deformations, an effective sensing system can be developed for damage location.

1.2 Motivation and Project Focus

This research is directed towards the exploration of a new application for structural health- monitoring with an old method of sensing. The approach was to model a sensor and determine the most appropriate design parameters. By integrating this into a TDR sensing system, a health-monitoring system can be designed for specific purposes from concrete structures to laminate polymer composites. The main examples in this thesis are concrete structures since there are so many examples of deteriorating civil structures as described in the introduction. The TDR system may have the advantage of being added to existing structures.

Four systems have been assembled for demonstration purposes at the Smart Materials Laboratory. Two were composed of Nitinol conductors, and the remaining systems used commercially available cables. As a group these demonstrations gave good responses to

external inputs (strain, temperature change, corrosion, and crack damage). The main delay in their application to real world situations was that there were no appropriate models to quantify the responses.

The first system was set up in 1989 to demonstrate the possibility of making a distributed sensor with Nitinol and TDR methods. Nitinol conductors were used because of their high resistance/strain and resistance/temperature relationships. The demonstration consisted of two Nitinol wires suspended in air and terminated by a resistor for an end reference point (see Figure 1.8). This sensor was attached to a Tektronix 1502-B TDR field unit. The system showed measurable responses to temperature and strain changes which were displayed as impedance changes. This demonstrated the advantages that the properly selected sensing materials may provide for a sensing cable.

The second system was composed of Nitinol wires embedded within an epoxy pull-out specimen. The specimen was part of an active damage control (ADC) project (Rogers, Liang, and Li, 1991). The wires were originally intended to reduce crack damage within the epoxy. When the wires were connected to an HP 54120 Digital Oscilloscope with TDR capabilities, they became an effective sensor for locating crack damage (see Figure 1.9). The initial TDR trace of the specimen was normalized to the signal given when stress was applied at the crack site. The difference in the normalized TDR signal was then used to evaluate crack growth. This demonstrated the capability to make the sensor an integral part of the structure.

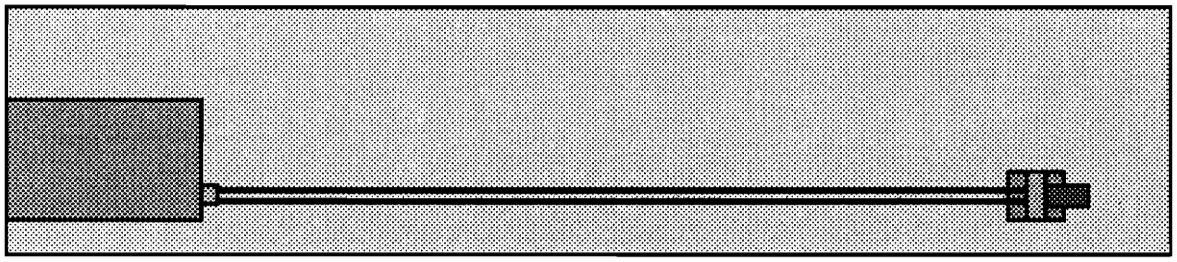

(a)

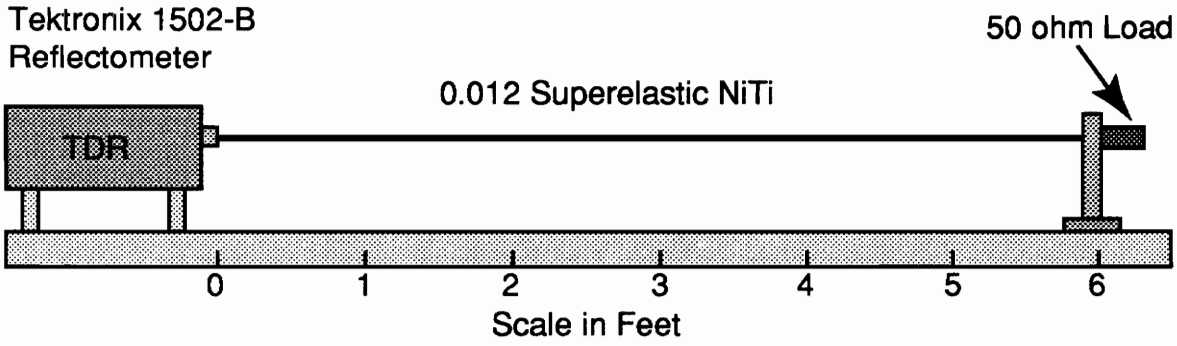

(b)

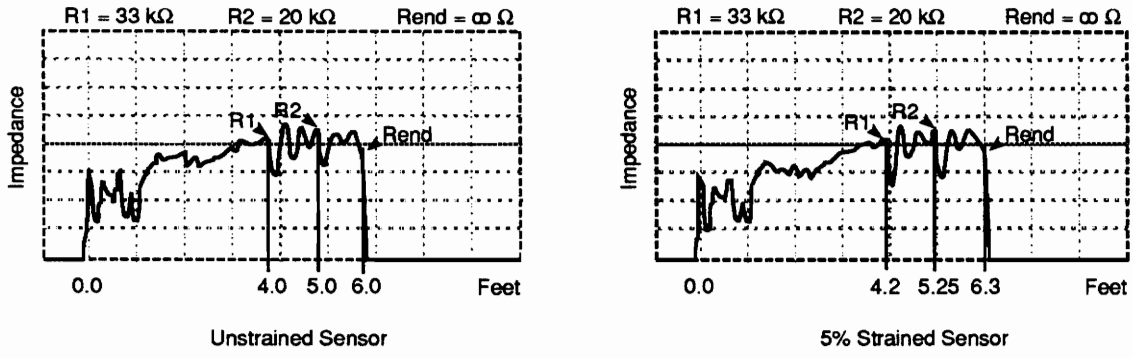

(c)

Figure 1.8 TDR set-up (a) topview, (b) sideview, and (c) test results for a strained sensor.

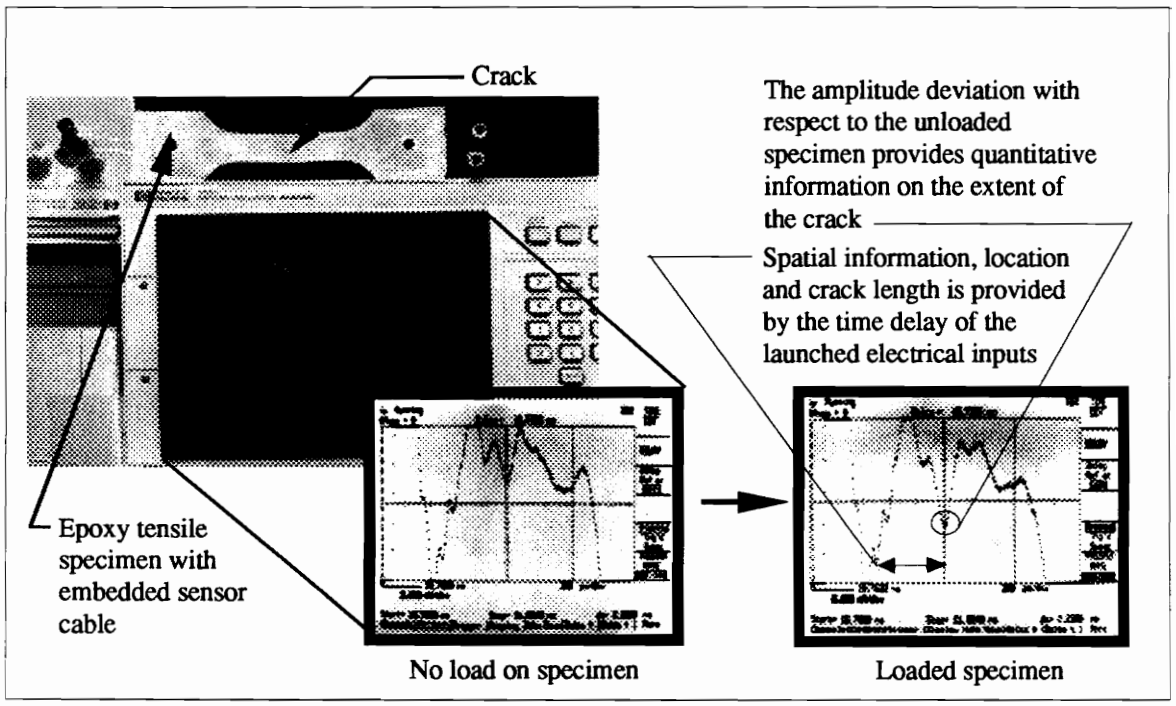

Figure 1.9 Epoxy and Nitinol wire specimen as a TDR sensor.

The third system used MM 330-DFV strain gage cable as the sensing element. As shown in Figure 1.10, the cable was shorted at one end and taped down to a table to keep random wire movements from occurring during the test. The short was used to determine the location of the end of the sensing cable. The other end was attached to the HP 54120. Location and intensity of a finger pressed upon the sensor wire were easily determined by both the real time TDR signal and the normalized TDR signal. The possible sensitivity of a properly designed health-monitoring system was demonstrated by this set-up.

The final system to date was used to evaluate corrosion. In this system, a 50 ohm coaxial cable was used as a sensor. The cable was mounted on a table top and then subjected to applications of hydrochloric acid (see Figure 1.11). The TDR signal was normalized to the original signal output and displayed an increase in the signal with subsequent applications of the acid. The system demonstrated the location and quantification of corrosion within and around the coaxial sensor.

These demonstrations have presented the possibilities for using a TDR oriented health monitoring system. The main body of this thesis provides the basis by which these methods can become a reality. By developing these design models, a system can be tailored to have the optimum sensing capabilities for the environment within which it will work. This idea of optimizing the design has been the motivation behind the work on

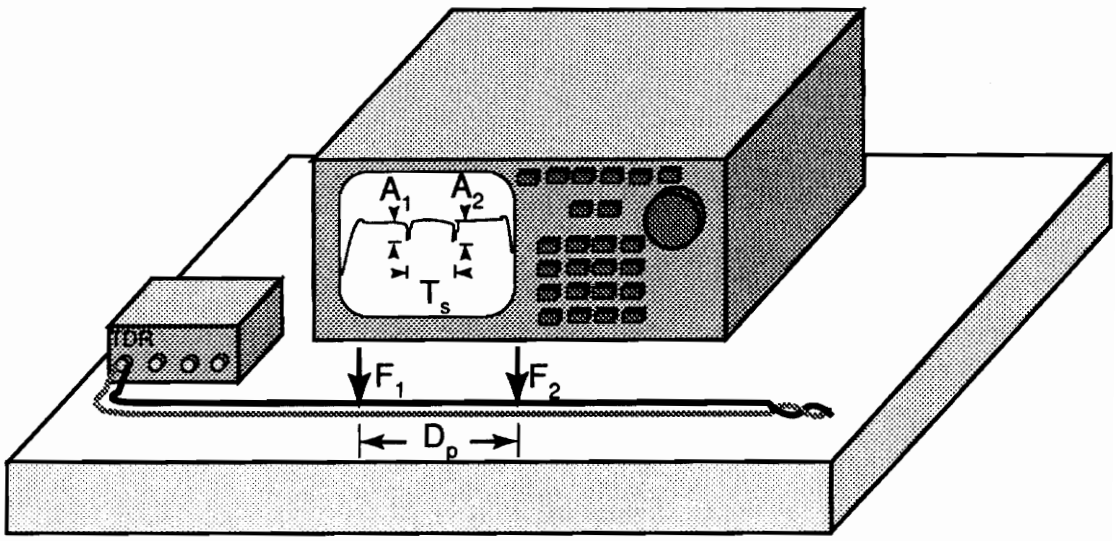

$$F_1 = K_F A_1 \qquad F_2 = K_F A_2$$

$$D_p = K_D T_s$$

Figure 1.10 TDR sensor with two-wire cable.

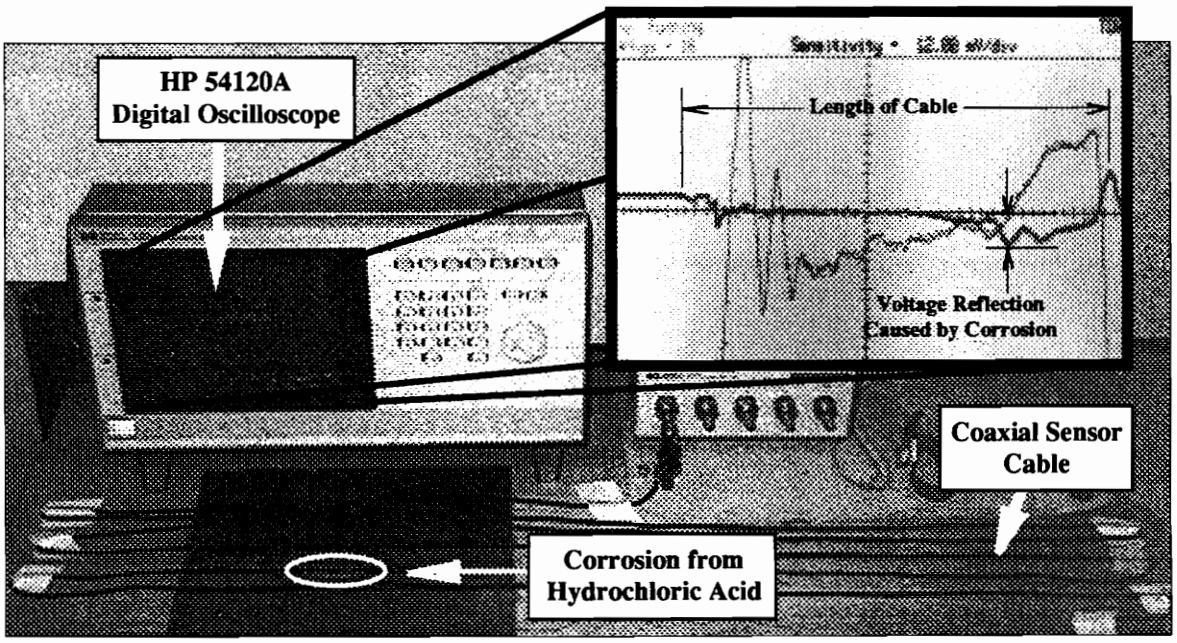

Figure 1.11 TDR corrosion sensor with 50 ohm coaxial cable.

this project.

1.3 Sensing Technologies for Civil Structures

TDR techniques have not been used specifically as civil structure sensors; however, researchers have developed the TDR techniques for other purposes which can be compared to present-day discrete sensors. These discrete sensors are in common use for concrete structure evaluation. Concrete, as described by Jones (1962), is a material which contains a large number of voids and has mechanical properties that are not accurately reproducible even under the best conditions. The goal behind using these sensing techniques is to provide a reliable estimate of the concrete quality in a structure without relying solely on results from test specimens which may not be representative of the structural concrete. To understand the present technology, it is good to have a description of how these particular sensors work and what the comparable TDR sensing technique is for different sensing priorities (temperature, stress, etc.). For this reason, the following sections give a brief discussion of the technology broken down by sensing priorities.

1.3.1 Temperature Sensors

Temperature fluctuations within a structure can be indicative of problem sites within that same structure. High strain sites, corrosion development, voids and cracks can be

located with careful heat flux analysis. A variety of devices have been used to obtain these type of measurements.

Various thermistors have been commercially available since 1971. They consist of thermally sensitive semiconductor elements sealed in a brass tube. The entire assembly is encased in thermoplastic before it is installed within the concrete. The leads from the thermistor are then attached to data acquisition equipment on the exterior of the concrete structure. The temperature at the embedded site can then be monitored for fluctuations. Several thermistors have to be installed to determine heat flow or to obtain the temperature distribution within the structure.

Infrared methods can be used and have been applied for nondestructive evaluation (NDE) of bridge decks. Photo equipment which is sensitive to the heat spectrum is used to diagram hot spots within the structure. Typically, this method is used for void evaluation since changes in heat flux can be related to high void sites. The major difficulties with this method are the disruption of traffic during evaluation periods and the detailed knowledge of characteristic heat flux for damage sites that is needed to determine normal heat flux within the structure.

Fiberoptic methods have been used in epoxy laminates. The refraction index is correlated to temperature changes within the fibers. A light source is placed at one end of the fibers and the refraction index changes due to the temperature will cause the

intensity of the light sensed at the other end of the fiber to change. This method has possible use in many structures, but the concrete environment is too harsh for the brittle fibers.

There has not been a comparable TDR technique for temperature evaluation. Work by Coleman (1990a) suggested the development of a distributed sensor using Nitinol wires that could have been adapted to temperature sensing. The Nitinol wires were used for their strong strain/resistance relationship, but they also have a temperature/resistance relationship which can be exploited. The wires were used as conductors in open air for a TDR sensor, but were never embedded within a structure to determine the sensitivity of an embedded system. More work in this area could lead to distributed temperature sensing.

1.3.2 Strain, Stress, and Pressure

Strain, stress, and pressure information is very important for monitoring structural health within concrete structures. Occurrences of large stress or strain sites are indicative of crack or fatigue damage. The typical sensing device employs a strain sensing component. Most of the commonly used concrete devices employ a metal with a strain-resistance relationship. Stress or pressure are then derived by a stress-strain relationship.

Embedded strain gages have been used in several different configurations. Weldable

gages are strain sensitive metal with some sort of serration or deformation which allows for bonding within the structure. Stress plugs involve embedding strain gages between a sample of the concrete and a waterproof coating, and placing the set-up within the concrete structure. The errors introduced by the differing properties of the plug and structural materials have been minimized to 0.5% for stresses up to 7000 psi for a period of one year (Coleman, 1990b). They are a custom fabrication and have been tested in the laboratory.

There are two types of sensors which use steel wire: vibrating wire strain gage and Carlson meters. The vibrating wire method has extensive use in thick-walled reactor vessels in Europe. It consists of a wire attached to a bellows. As the bellows is activated, the wire tension changes. An actuation and sensing device causes the wire to vibrate and measures the change in the vibration as the gage is strained. It has been tested to 0.1 microstrain resolution, but drift is a problem. The chief disadvantage is the high cost of manufacture and use. The vibrating wire sensors been commercially available since 1983. Carlson meters use the change in resistance of two steel wire coils prestressed at 100,000 psi which shift in equal amounts but opposite directions. Strain gage type circuitry is used to get 5 microstrain resolution or up to 0.1 degree F total temperature change when suitably embedded. Carlson meters have been commercially available since the late sixties.

The use of load washers is another method for stress measurement. One method uses

a microducer as a load washer. The microducer is composed of a stress sensitive paint squeezed between metal washers with electric leads. It is used for measuring small loads. Another method uses elastic tabs. The tabs are calibrated so that when they are compressed, the load can be determined from the measured displacement. This method is used to measure large loads. Both washers are commercially available.

Acoustic emission has also been used to locate high stress or strain sites. Through the use of a striker and a receiver, the acoustic impedance of the structure can be evaluated over its surface. The stress or strain sites will give an acoustical signal which varies from the normal acoustics. Ouyang et. al. (1991) have implemented a truck mounted system. The main disadvantage is that the system does not constantly monitor the condition of the structure. Another hindrance is that the object under inspection must be cleared of other vehicles, therefore traffic is disrupted while the inspection occurs.

Fiberoptic methods are similar to those used for temperature measurement. The difference is that the index of refraction is related to stress rather than temperature. The brittleness of the fibers is still a problem. Much of this work is developed from custom laboratory fabrications.

Su (1987) has developed a method for using TDR sensing in monitoring rock wall damage. He and others (Dowding, O'Connor and Su, 1989) have applied this method to monitoring caving walls in coal mining operations. Their method used grouting

material (40-65% water, 2% Intrusion Aid, and the rest is Portland cement) to surround the sensor cable (standard coaxial cable). Shear and linear strain data were obtained and mining wall crack propagation was monitored by the system. By using this method within concrete structures, a damage detection system can be developed for civil structures.

1.3.3 Moisture

Moisture is a significant concern in concrete structures. The material strength can be seriously degraded by moisture penetration or improper cure. Few techniques exist to measure moisture content. Most of these rely on the conductivity of concrete as a function of its moisture content. The resistance is measured between a set of electrodes. For cases where the resistance between the electrodes and the concrete (contact resistance) is not negligible, a moisture gage is embedded within a moisture absorbent material and then the entire system is inserted in the concrete.

Another technique which has been used to determine water content within concrete is microwave reflection or transmission measurements. A microwave transducer sends out microwave pulses. The pulses are directed at the concrete inspection site and either the reflected pulses or the transmitted (depending upon access to the site) are recorded for analysis. The signals are compared to the pulses that are received when a practically perfect reflector (a metal sheet) is placed over the same area of concrete. The data is

calibrated against concrete with a known water content. The majority of this work has been used to analyze fresh concrete in a laboratory environment (Clemeña, 1987), but it could develop into a plausible method for determining water content within concrete structures. The main limitation is that the structure must be accessible to the inspection equipment.

Moisture within the structures can lead to corrosion. Interesting work in this field has been done by Dry (1992). The work involves the use of chemical sensors which will release anticorrosion chemicals when corrosion is evident. The same research has explored the use of embedded fibers which can be used to apply the chemicals at the site of corrosion and also apply bonding materials to deter crack propagation.

In the TDR field, soil water content has been explored by Topp, Davis, and Anan (1980). A sensor cable was inserted into the soil and then monitored with TDR data acquisition equipment. The cable impedance changed with the water content of the surrounding soil. An expansion of their work could be applied to civil structures if correlations between water content and impedance are developed for cables within concrete structures.

The history of the human race is a continuous struggle from darkness toward light. It is therefore of no purpose to discuss the use of knowledge - man wants to know and when he ceases to do so he is no longer man...

- Fridt Jof Nansen, Early Twentieth Century

Chapter 2

Background Theory

In this chapter, a discussion and derivation of the theory which is the basis for this project is given. The development of the potential function from Coulomb's Law is demonstrated and a description is given of the impedance relationships to the potential function. The majority of this work is a review of work presented by Neff (1981). More detailed material may be found in Elmore (1975) and Sinnema (1979). Finally, the background of the parametric equations for the models of Chapter 3 are derived for the coaxial and the two-wire cases. The derivation of the single dielectric equations are typical textbook problems considered in the previously mentioned texts; however, the development for a two dielectric case is this author's attempt at describing behavior with the different boundary conditions.

2.1 The Potential Function

Coulomb's Law states that the force between two fixed small charged objects, with charges Q_1 and Q_2, in a vacuum is directly proportional to Q_1 and Q_2, and inversely

proportional to the square of the distance (R) between the charges, or written as

$$F = K \frac{Q_1 Q_2}{R^2} \quad . \tag{2.1}$$

This is represented in Figure 2.1 where

$$R = | \vec{r}_2 - \vec{r}_1 | = \sqrt{(x_2 - x_1)^2 + (y_2 - y_1)^2 + (z_2 - z_1)^2} \quad . \tag{2.2}$$

Once the charges are in their respective places, an external force will be required to oppose the Coulomb force and keep the charged objects in a given position. Additional force brought on by external work (negative or positive) will also oppose that given by Coulomb's Law.

An electric field is defined as the force on a unit positive charge; therefore, the force on any point charge Q in an arbitrary field is

$$\vec{F} = Q\vec{E} \quad (N) \quad . \tag{2.3}$$

This force must be overcome if an external force is to move the charge Q. If the charge is to move an incremental distance $\Delta \mathbf{l}$ vector where

$$\Delta \vec{l} = \vec{a}_l \, \Delta l \quad , \tag{2.4}$$

the component force to be overcome is

$$\vec{F} \bullet \vec{a}_l = Q\vec{E} \bullet \vec{a}_l \quad (N) \quad . \tag{2.5}$$

The external scalar force is

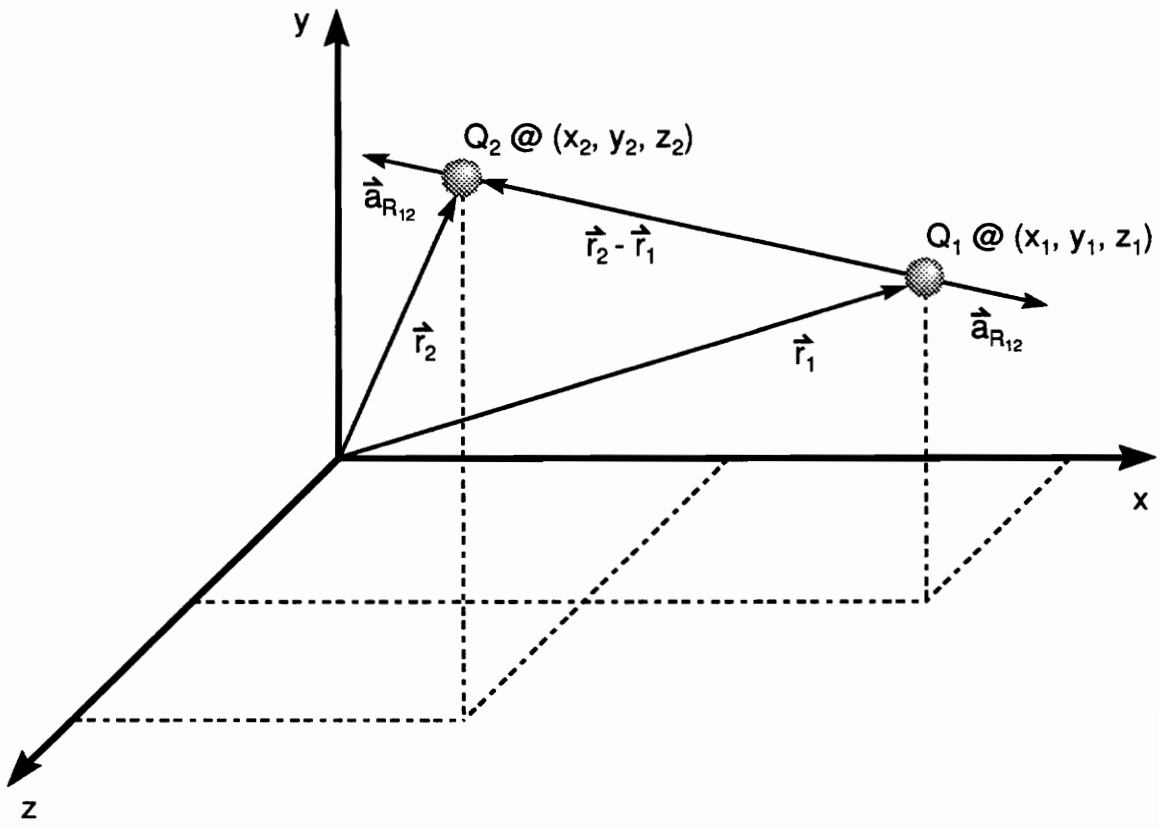

Figure 2.1 Coulomb's Law

$$F_{ext} = -Q\vec{E} \bullet \vec{a}_l \quad (N) \quad . \tag{2.6}$$

Work is force times distance, so the incremental work done by the external force is

$$\Delta W = Q\vec{E} \bullet \vec{a}_l \, \Delta l = -Q\vec{E} \bullet \Delta\vec{l} \quad (J) \quad . \tag{2.7}$$

If the external force moves the point charge from a point P_i to a final point P_f along a path C (see Figure 2.2), the total work required can be approximated as a finite sum of incremental amounts of work as shown in the following equation:

$$W \approx -Q\sum_{n=1}^{N} \vec{E}_n \bullet \Delta\vec{l}_n \quad (J) \quad . \tag{2.8}$$

For this equation, $\mathbf{E_n}$ is the electric field intensity at the nth point on the path. If N approaches infinity in such a way that the incremental distance at n approaches zero for any n, the limit is an exact integral expression for W. The resulting line integral is

$$W = -Q\int_{P_i}^{P_f} \vec{E} \bullet d\vec{l} \quad (J) \quad . \tag{2.9}$$

The electrostatic electric field **E** is a special field which allows the preceding integral to be independent of the path. For the line integrals that will be encountered, the incremental distance **dl** is

$$d\vec{l} = \vec{a}_x \, dx + \vec{a}_y \, dy + \vec{a}_z \, dz \tag{2.10}$$

in Cartesian coordinates,

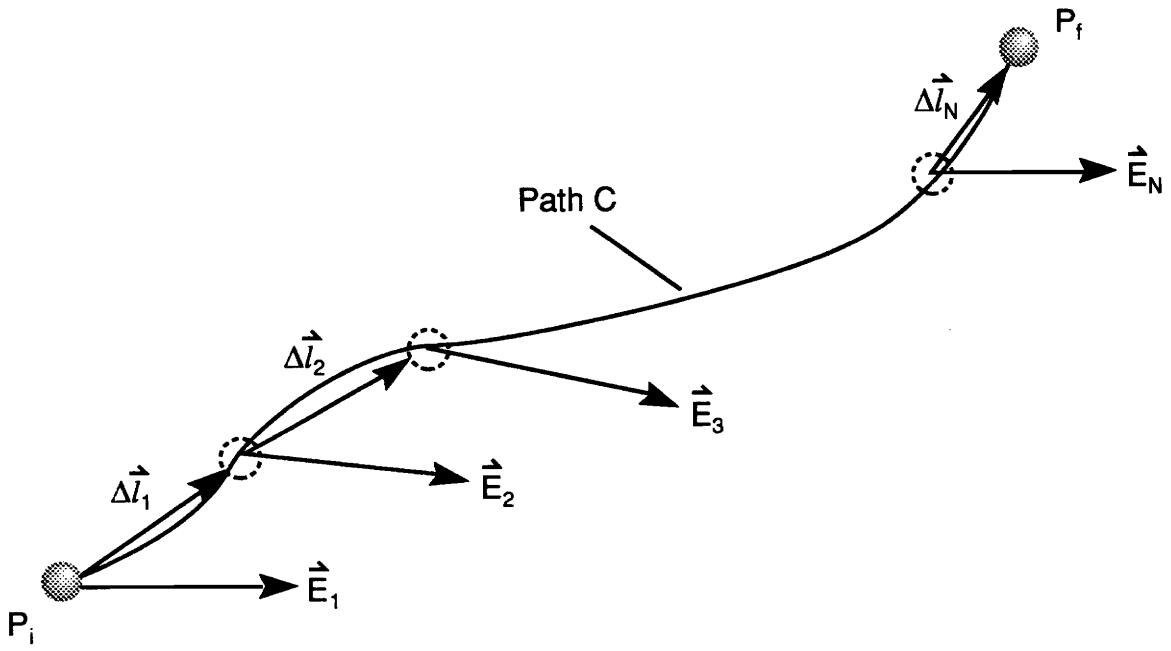

Figure 2.2 Point Charge on Path C

$$d\vec{l} = \vec{a}_\rho \, d\rho + \vec{a}_\phi \, \rho d\phi + \vec{a}_z \, dz \qquad (2.11)$$

in cylindrical coordinates, and

$$d\vec{l} = \vec{a}_r \, dr + \vec{a}_\theta \, r d\theta + \vec{a}_\phi \, r \sin\theta d\phi \qquad (2.12)$$

in spherical coordinates.

It must be recognized that the sign of dl is not an arbitrary parameter. The direction along the path of integration is taken care of by the limits on the integral, P_i and P_f. The potential difference between P_i and P_f is the work required by an external source to move a unit positive charge from P_i to P_f in the field E. This is the previous work equation with a charge Q = 1:

$$\phi_{fi} = \phi_f - \phi_i = -\int_{P_i}^{P_f} \vec{E} \bullet d\vec{l} \qquad (J/C = V) \quad . \qquad (2.13)$$

In the electrostatic case, the potential difference ϕ_{fi} is the same as the voltage difference of circuit theory. The potential difference is also equal to the absolute potential (ϕ_f) at point P_f minus the absolute potential (ϕ_i) at point P_i. The absolute potential at a point $\phi(x,y,z)$ is the potential difference between that point and some reference point where the potential is zero and called "ground".

An example of a line charge (infinite length, uniform with charge density ρ_l (C/m)) with a field that is

$$\vec{E} = \frac{\rho_l}{2\pi\epsilon_0\rho}\vec{a}_\rho \quad , \tag{2.14}$$

will be the starting point of the derivation for ϕ_{fi} with two dielectric constants. First, the derivation for one dielectric constant (ϵ_0) must be developed.

2.1.1 Potential Function in Uniform Dielectric Medium

The potential difference between P_f and P_i which are lying along a cylindrical radial line (ϕ(r),z = constant) at radii a and b (b > a) is:

$$\phi_f - \phi_i = \phi(a) - \phi(b) = -\int_b^a \vec{E} \bullet d\vec{l} \tag{2.15}$$

$$\phi(a) - \phi(b) = -\int_b^a \frac{\rho_l}{2\pi\epsilon_0\rho}\vec{a}_\rho \bullet \vec{a}_\rho \, d\rho = -\frac{\rho_l}{2\pi\epsilon_0}\int_b^a \frac{d\rho}{\rho} \tag{2.16}$$

$$\phi(a) - \phi(b) = -\frac{\rho_l}{2\pi\epsilon_0}\ln\rho \Big|_b^a \quad , \tag{2.17}$$

so

$$\phi(a) - \phi(b) = -\frac{\rho_l}{2\pi\epsilon_0}(\ln a - \ln b) \quad , \tag{2.18}$$

and

$$\phi(a) - \phi(b) = \frac{\rho_l}{2\pi\epsilon_0} \ln \frac{b}{a} \quad (V) \quad . \tag{2.19}$$

Since b > a (refer to Figure 2.3), the potential difference is positive. As b approaches infinity, ϕ_{fi} becomes infinite, therefore a cylinder of infinite radius is not a suitable reference for absolute potential. This can be overcome in a general way if ϕ(r) is defined as

$$\phi(r) = -\int_l \vec{E} \bullet dl + K \quad , \tag{2.20}$$

where K is chosen to be whatever reference that is desired. The electric field for an infinite line charge (Equation 2.14) can be substituted into Equation 2.20 to give

$$\phi(\rho) = -\frac{\rho_l}{2\pi\epsilon_0} \ln \rho + K \quad . \tag{2.21}$$

If K is chosen such that $\phi(\rho) = 0$ when $\rho = 1$, then K = 0 and

$$\phi(\rho) = -\frac{\rho_l}{2\pi\epsilon_0} \ln \rho \tag{2.22}$$

for any ρ. The equipotential surfaces are cylinders coaxial with the line charge. The example can now be written as

$$\phi(a) - \phi(b) = -\frac{\rho_l}{2\pi\epsilon_0} (\ln a + K - \ln b - K) = \frac{\rho_l}{2\pi\epsilon_0} \ln \frac{b}{a} \quad , \tag{2.23}$$

which shows that the absolute potential is arbitrary to an additive constant K.

This derivation can now be used to determine the potential within a uniform dielectric

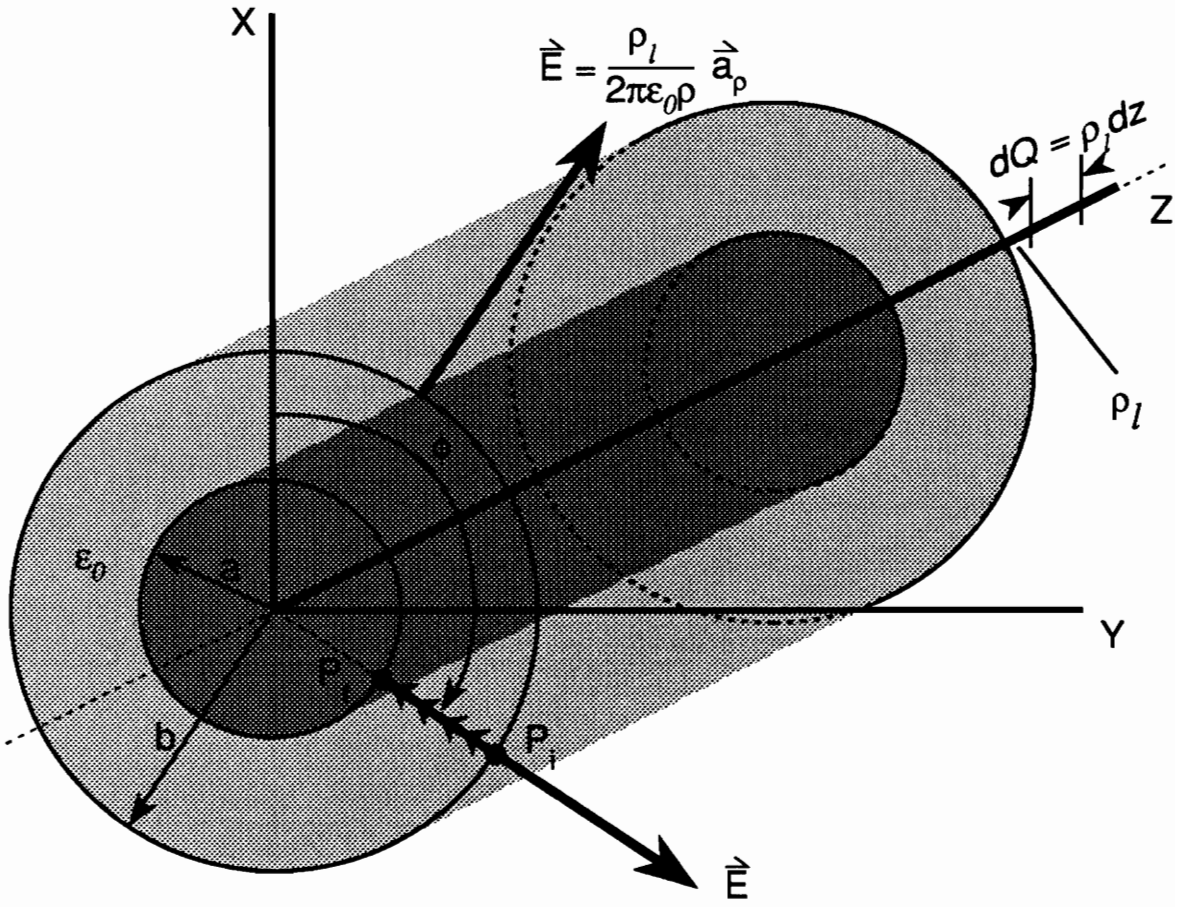

Figure 2.3 Equipotentials for Uniform Dielectric

for various geometries. The coaxial geometry is solved by applying flux boundary conditions. The two-wire cable is solved through the use of superposition on a symmetrical plane. The following derivation covers the problem of having a medium with two dielectric constants.

2.1.2 Potential within a Two Dielectric Medium

The potential derivation for a medium with two dielectric constants, ϵ_1 and ϵ_2, follows closely to that of a uniform dielectric. Once again, there is an infinite line charge of uniform charge density ρ_l (C/m) in an electrostatic field:

$$\vec{E} = \frac{\rho_l}{2\pi\epsilon\rho}\vec{a}_\rho \quad . \tag{2.24}$$

The dielectric constant varies for this example and must be considered within the solution of the forthcoming integral. Figure 2.4 demonstrates the similarity of the model geometry to that of uniform dielectric (compare to Figure 2.3).

The potential difference between points P_f and P_i along a radial line at radii a and b (b > a) is again

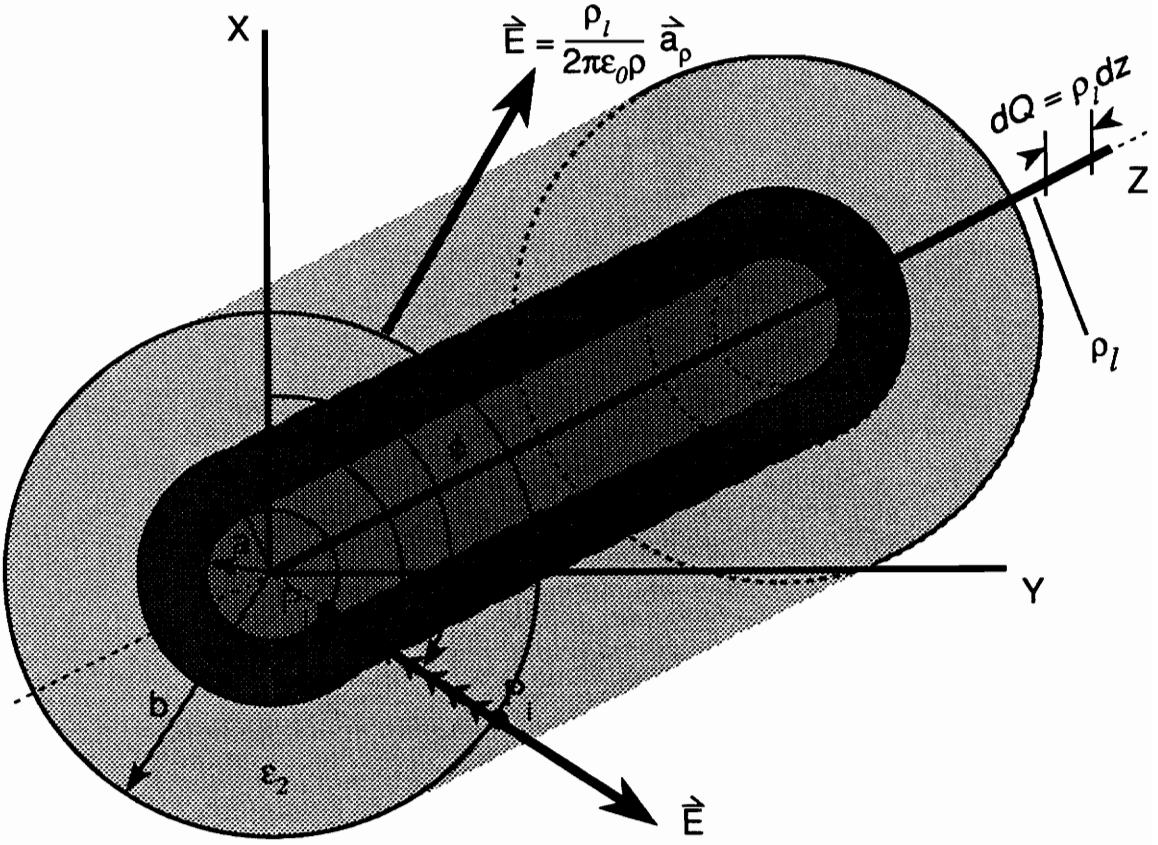

Figure 2.4 Equipotentials for a Two Dielectric Medium

$$\phi_f - \phi_i = \phi(a) - \phi(b) = -\int_b^a \vec{E} \bullet d\vec{l} \quad . \tag{2.25}$$

To accommodate the change in dielectric properties at radius e, the behavior of the flux density must be examined. The flux density **D** is the charge divided by the area through which it flows. The radial component of the flux density D_ρ must remain constant through a property change such as the one shown in Figure 2.5 for a line charge ρ_l. This requirement gives

$$D_{1\rho} = D_{2\rho} \quad . \tag{2.26}$$

The flux density is then related to the electric field by the dielectric constant ϵ such that

$$\vec{D} = \epsilon \vec{E} \quad . \tag{2.27}$$

The radial flux density and electric field equations on each side of the dielectric discontinuity are

$$D_{1\rho} = \epsilon_1 E_{1\rho} \quad , \tag{2.28}$$

and

$$D_{2\rho} = \epsilon_2 E_{2\rho} \quad . \tag{2.29}$$

Equations 2.28 and 2.29 are substituted into Equation 2.26 to give

$$\epsilon_1 E_{1\rho} = \epsilon_2 E_{2\rho} \quad . \tag{2.30}$$

For a known electrostatic field ($E_{1\rho}$) generated by the line charge ρ_l, the corresponding

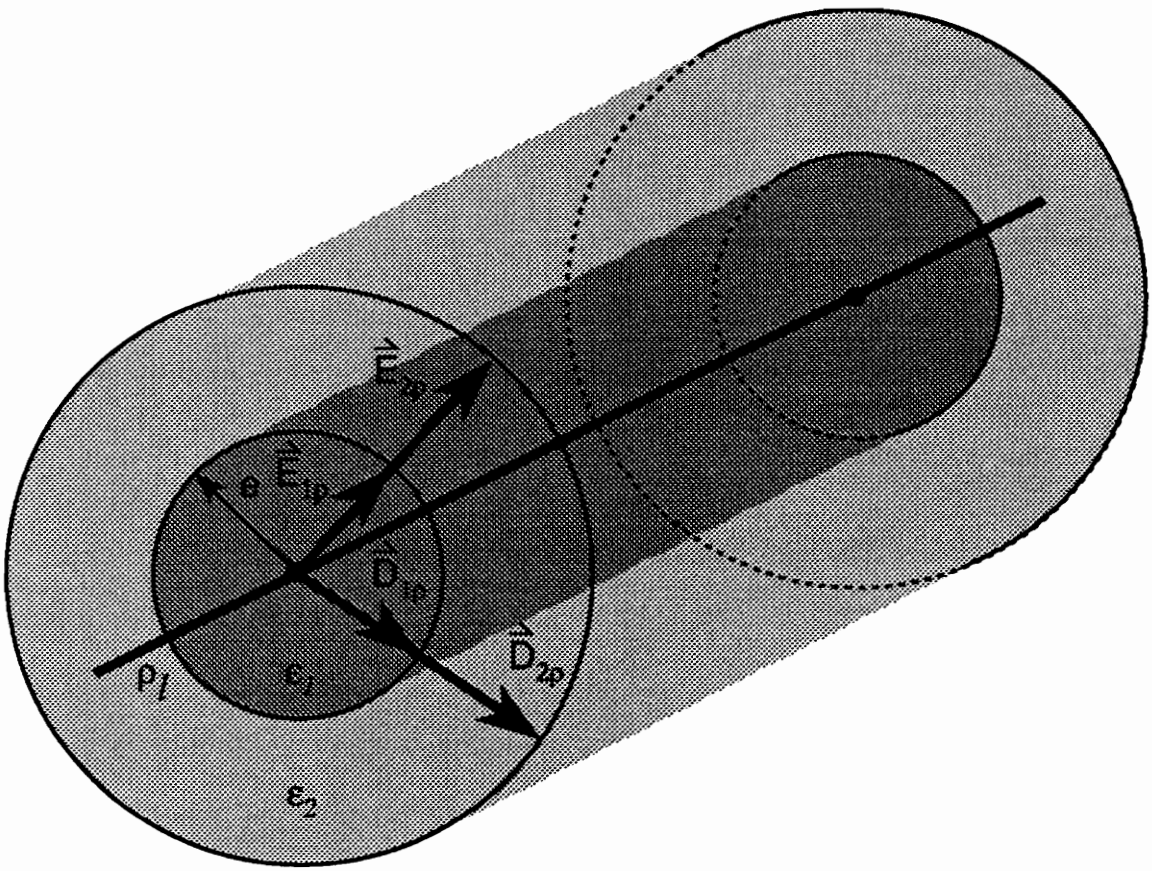

Figure 2.5 Flux Density at a Discontinuity

field across the discontinuity will be

$$E_{2\rho} = \frac{\epsilon_1}{\epsilon_2} E_{1\rho} \quad . \tag{2.31}$$

This gives the radial component for a cylindrical field as

$$E_{2\rho} = \frac{\epsilon_1}{\epsilon_2} \frac{\rho_l}{2\pi\epsilon_1\rho} = \frac{\rho_l}{2\pi\epsilon_2\rho} \quad . \tag{2.32}$$

Now the potential difference integral is

$$\phi(a) - \phi(b) = -\int_b^a E_\rho \vec{a}_\rho \bullet \vec{a}_\rho \, d\rho = -\int_b^a E_\rho d\rho \quad . \tag{2.33}$$

The field changes at radius e, so the integral from b to a must be separated into a sum from b to e and from e to a such that

$$\phi(a) - \phi(b) = -\int_b^e E_\rho d\rho - \int_e^a E_\rho d\rho \quad . \tag{2.34}$$

Now the two field components ($E_{1\rho}$ and $E_{2\rho}$) can be substituted into the potential difference equation:

$$\phi(a) - \phi(b) = -\int_b^e \frac{\rho_l}{2\pi\epsilon_2\rho} d\rho - \int_e^a \frac{\rho_l}{2\pi\epsilon_1\rho} d\rho = -\frac{\rho_l}{2\pi}\left[\frac{1}{\epsilon_2}\int_b^e \frac{d\rho}{\rho} + \frac{1}{\epsilon_1}\int_e^a d\rho\right] . \tag{2.35}$$

The integral solutions can then be determined as

$$\phi(a) - \phi(b) = -\frac{\rho_l}{2\pi}\left[\frac{1}{\epsilon_2}\ln\rho\Big|_b^e + \frac{1}{\epsilon_1}\ln\rho\Big|_e^a\right] \quad ; \tag{2.36}$$

then

$$\phi(a) - \phi(b) = -\frac{\rho_l}{2\pi}\left[\frac{1}{\epsilon_2}(\ln e - \ln b) + \frac{1}{\epsilon_1}(\ln a - \ln e)\right] \quad ; \tag{2.37}$$

and finally,

$$\phi(a) - \phi(b) = \frac{\rho_l}{2\pi\epsilon_2}\ln\frac{b}{e} + \frac{\rho_l}{2\pi\epsilon_1}\ln\frac{e}{a} \quad . \tag{2.38}$$

This equation is very much like the previous derivation of Equation 2.21, except for the change that takes place at radius e. The equations are now written as

$$\phi(\rho) = -\frac{\rho_l}{2\pi\epsilon_1}\ln\rho + K_1 = -\frac{\rho_l}{2\pi\epsilon_1}\ln\frac{\rho}{e} \quad , \tag{2.39}$$

for $\rho < e$, and

$$\phi(\rho) = -\frac{\rho_l}{2\pi\epsilon_2}\ln\rho + K_2 = -\frac{\rho_l}{2\pi\epsilon_2}\ln\frac{\rho}{e} \tag{2.40}$$

for $\rho > e$.

The upper bound and the lower bound equations are now determined for a two dielectric medium. These equations still rely on constants to define a reference for absolute potentials. Without the constants (K_1 and K_2), the potential difference at infinity is infinite.

2.2 Impedance Property Relationships

It is helpful to explain the importance of an appropriate potential difference equation. This one function can be related to three of the relevant terms in the impedance equation

$$Z = \sqrt{\frac{R+i\omega L}{G+i\omega C}} \quad . \tag{2.41}$$

The conductance G, inductance L, and capacitance C can all be related to the potential difference equation ϕ_{fi}. The resistance R of the conductors can easily be added by using the conductor geometry and resistivity.

The derivation of the potential difference relationships begins with the capacitance of the transmission system. The system (shown in Figure 2.6) is based on two conductors in a dielectric medium. The capacitance of this system is defined as the ratio of the total charge on the positive charged conductor to the potential difference ϕ_{ab} between the two conductors, and is made a positive quantity by putting point a on the positive charged conductor. This also makes the potential difference ϕ_{ab} positive:

$$C = \frac{Q_a}{\phi_{ab}} \qquad (F/m) \quad . \tag{2.42}$$

Through the use of Gauss' Law, the equation can be written as

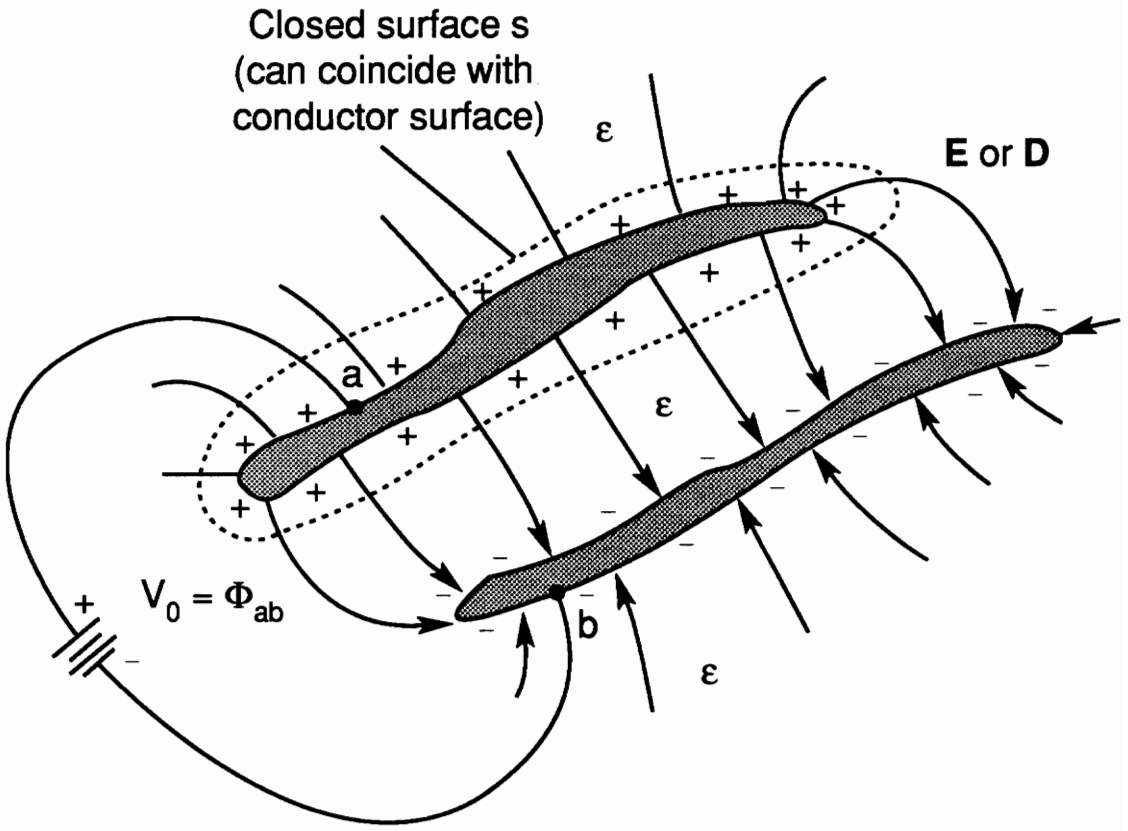

Figure 2.6 Capacitive System

$$C = \frac{\oint_S \epsilon \vec{E} \cdot d\vec{s}}{\phi_{ab}} = \frac{-\oint_S \epsilon \nabla\vec{\phi} \cdot d\vec{s}}{\phi_{ab}} \quad . \tag{2.43}$$

Equation 2.43 can be useful when numerical methods are used to calculate the potential. The conductance of this model is based upon the resistance of the medium in which the conductors are evident. Conductance is the inverse of resistance and can be defined as

$$R \equiv \frac{\phi_{ab}}{I} = \frac{1}{G} \quad (\Omega\ /m) \quad . \tag{2.44}$$

The conductance system is similar to our previous system where **J** is the conduction current density and σ is the conductivity (see Figure 2.7). The conductance can then be written for the closed surface s as

$$G = \frac{\oint_S \sigma \vec{E} \cdot d\vec{s}}{\phi_{ab}} = \frac{-\oint_S \sigma \nabla\vec{\phi} \cdot d\vec{s}}{\phi_{ab}} \quad (S/m) \quad . \tag{2.45}$$

Resistance and conductance are defined as positive quantities and will only depend on geometry and σ. By comparing the capacitance and conductance equations, it is seen that if σ and ϵ have the same dependance on position, C will be proportional to G for the same geometries. If σ and ϵ are constants, then

$$\frac{C}{G} = \frac{\epsilon}{\sigma} \quad . \tag{2.46}$$

The inductance derivation is also related to the capacitance and based on similar

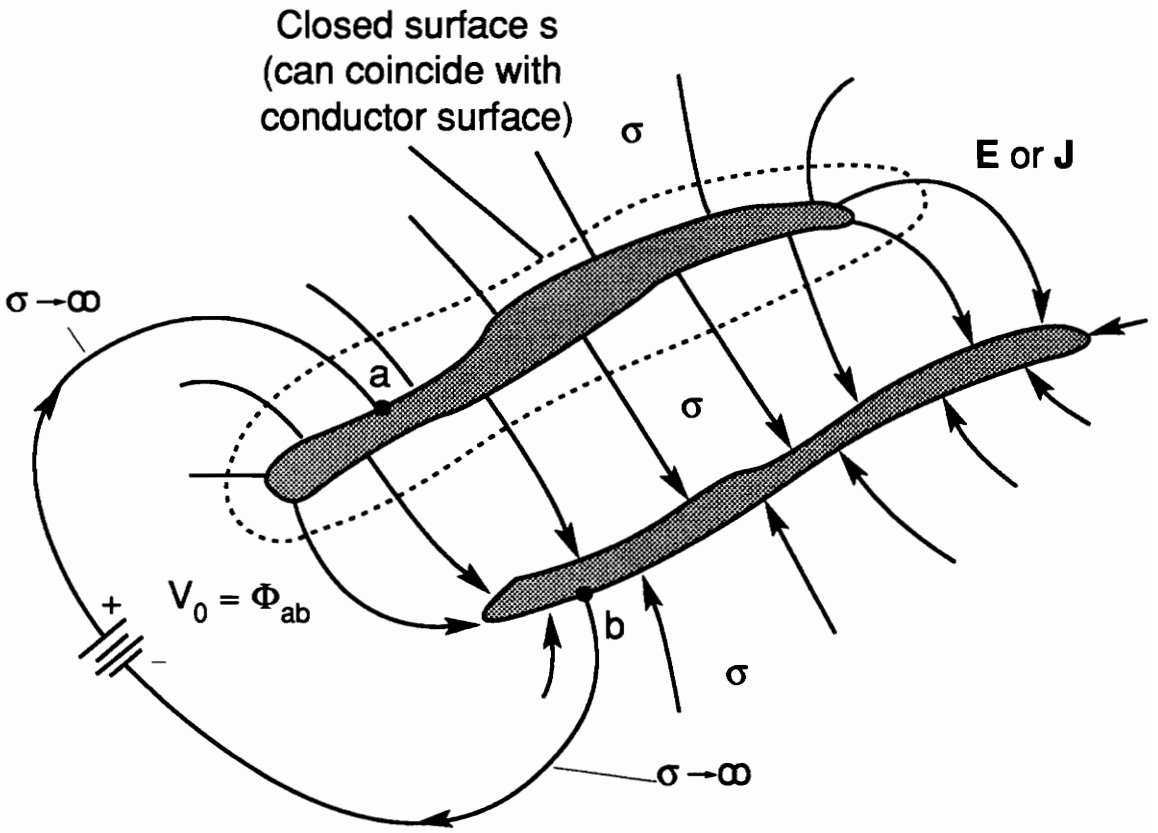

Figure 2.7 Conductance System

geometries. For these derivatives, **H** is the magnetic field intensity, **B** is the magnetic flux density, and ϕ_m is the magnetic potential. The similarities between a magnetic system and an electric system are evident from Figures 2.8 a and b respectively. From these systems the equations for capacitance

$$C = \frac{\epsilon \oiint_b \vec{E} \bullet d\vec{s}}{\int_{d,c_1} \vec{E} \bullet d\vec{l}_1} = \frac{\epsilon \oint_{c_2} E_n dl_2}{\int_{d,c_1} E_n dl_1} \quad (F/m) \quad , \tag{2.47}$$

and for inductance

$$L_{ext} = \frac{\mu \oiint_b \vec{H} \bullet d\vec{s}}{\oint_{c_2} \vec{H} \bullet d\vec{l}_2} = \frac{\mu \int_{d,c_1}^{b} H_t dl_1}{\oint_{c_2} H_t dl_2} \quad (H/m) \tag{2.48}$$

are developed. By multiplying these two equations and using $E_n = KH_t$, the resulting equation is

$$L_{ext} C = \frac{\mu \int_{d,c_1}^{b} H_t dl_1}{\oint_{c_2} H_t dl_2} \frac{\epsilon K \oint_{c_2} H_t dl_2}{K \int_{d,c_1}^{b} H_t dl_1} \quad , \tag{2.49}$$

which can be simplified to

$$L_{ext} C = \mu \epsilon \quad . \tag{2.50}$$

The inductance L_{ext} can now be calculated if C is known.

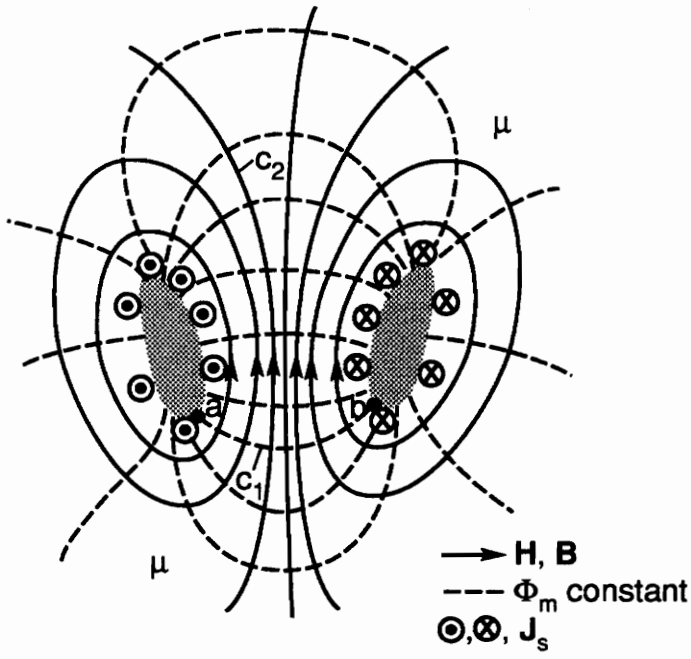

(a)

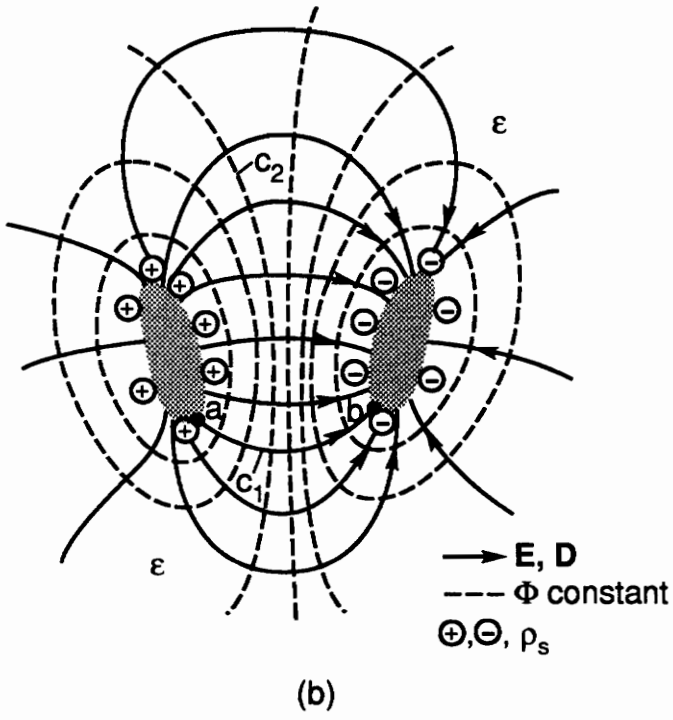

(b)

Figure 2.8 (a) Magnetic Potential System (b) Electric Potential System

2.2.1 Capacitance for a Coaxial Cable

The capacitance for a coaxial cable can be determined by using a Gaussian surface. These methods also demonstrate that this system is shielded from external electromagnetic fields.

Gauss's Law states that, "The electric flux passing through any closed surface is equal to the charge enclosed by that surface." Simply stated, the flux out equals the net charge enclosed, or

$$\Psi_E = Q \quad . \tag{2.51}$$

The flux out is obtained by integrating the differential flux at a point on the closed surface. This is represented by

$$\Psi_E = \oiint_s D|_s \cdot ds \quad , \tag{2.52}$$

where $\mathbf{D}|_s$ is the flux at point s and ds is outwardly normal to the Gaussian surface at point s.

The net charge enclosed can be obtained by integrating the charge density within the volume included by the Gaussian surface. This gives

$$Q = \iiint_{Vol} \rho_v dv \quad , \tag{2.53}$$

and Gauss's Law can then be mathematically represented as

$$\oiint_s D|_s \cdot ds = \iiint_{Vol} \rho_v dv \quad . \tag{2.54}$$

The coaxial cable is composed of two coaxial cylinders, one of outer radius a and one of inner radius b, with a dielectric material between them (see Figure 2.9). When a potential ϕ_{ab} is applied across the conductors, a charge is created on the conductors. The total charge on the inner conductor for a length L will be

$$Q = 2\pi a L \rho_{sa} \quad , \tag{2.55}$$

and the total charge on the outer conductor will be

$$-Q = 2\pi b L \rho_{sb} \quad . \tag{2.56}$$

If the coaxial is considered to be very long, the end effects will be negligible and the symmetry will be the same as that for a uniform line charge. The electric field is also the same, and is dependent on radius ρ or written as

$$\vec{E} = \vec{a}_\rho E_\rho(\rho) \quad . \tag{2.57}$$

By using a cylinder of radius ρ that is coaxial with the conductors as a Gaussian surface, the coaxial cable system is shown to be shielded such that

$$E_\rho = 0 \quad for \; 0 \leq \rho < a \quad and \quad for \; \rho > b. \tag{2.58}$$

Gauss's Law will then give

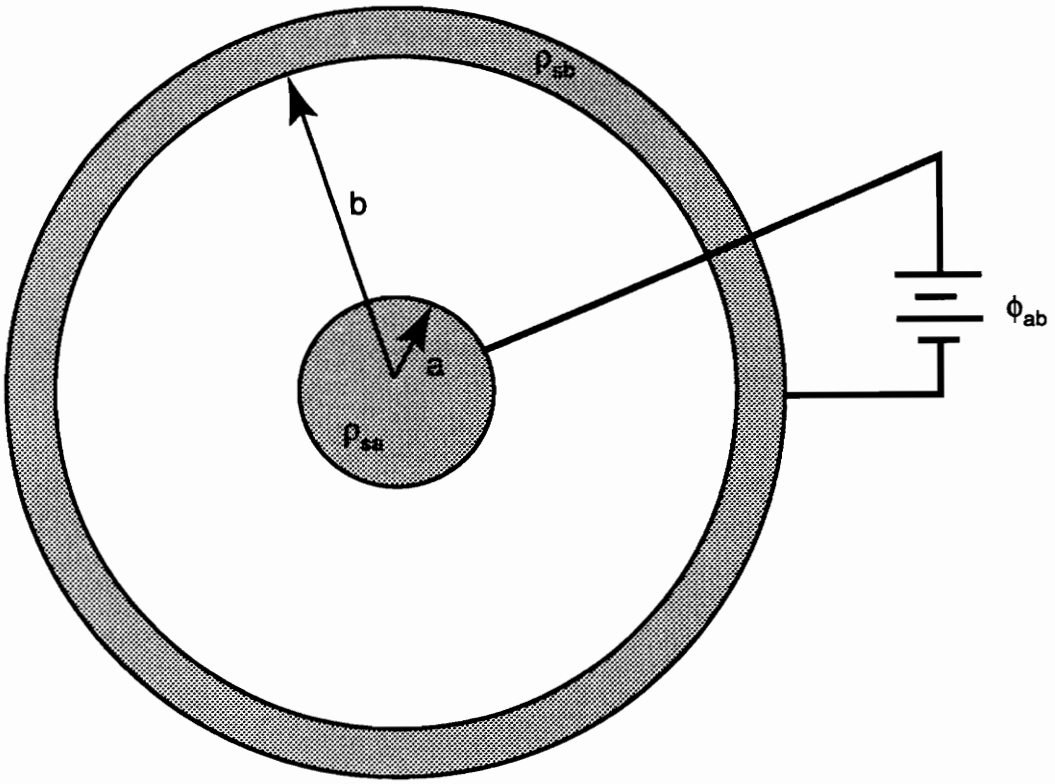

Figure 2.9 Capacitance in a coaxial system.

$$\Psi_E = D_\rho \int_0^L \int_0^{2\pi} \rho \, d\phi \, dz = Q_{enc} = 2\pi a L \rho_{sa} \quad , \tag{2.59}$$

and

$$D_\rho 2\pi\rho L = 2\pi a L \rho_{sa} \quad , \tag{2.60}$$

and finally,

$$D_\rho = \frac{a}{\rho}\rho_{sa} \quad . \tag{2.61}$$

The electric field for flux D_ρ within a dielectric material with permittivity ϵ will be

$$E_\rho = \frac{a\rho_{sa}}{\rho\epsilon} \quad . \tag{2.62}$$

The potential is then derived as

$$\phi = -\int E_\rho d\rho + K_1 = \frac{a\rho_{sa}}{\epsilon}\int -\frac{d\rho}{\rho} + K_1 \quad , \tag{2.63}$$

and

$$\phi = -\frac{a\rho_{sa}}{\epsilon}\ln\rho + K_1 \quad . \tag{2.64}$$

From the previous equations $\phi = 0$ when $\rho = b$, so

$$\phi = -\frac{a\rho_{sa}}{\epsilon}\ln\rho/b = \frac{a\rho_{sa}}{\epsilon}\ln b/\rho \quad ; \tag{2.65}$$

and since $\phi = V_0 = \phi_{ab}$ when $\rho = a$, the potential becomes

$$\phi_{ab} = -\frac{a\rho_{sa}}{\epsilon} \ln b/a \quad . \tag{2.66}$$

The total capacitance for this cable will be

$$C = \frac{Q}{\phi_{ab}} = \frac{2\pi a L \rho_{sa}}{(a\rho_{sa}/\epsilon)\ln(b/a)} \quad ; \tag{2.67}$$

or, in another way,

$$C = \frac{2\pi\epsilon L}{\ln(b/a)} \quad (F) \quad . \tag{2.68}$$

The capacitance per unit length is then

$$C = \frac{2\pi\epsilon}{\ln(b/a)} \quad (F/m) \quad . \tag{2.69}$$

The impedance per unit length can now be derived by using the capacitance equation and the impedance relationships described in the introduction to Section 2.2.

2.2.2 Capacitance for a Two-Wire Line

Capacitance for a two-wire line is determined from the potential function for a single line charge. The solution is obtained by superposition of the two individual charges onto each other. If both line charges are made to exist at the same time, the electric fields are known to be additive. The total field is given by

$$\vec{E} = \vec{E}_1 + \vec{E}_2 \quad . \tag{2.70}$$

The potential is derived from the field intensity by line integration. The potentials also

superimpose since the integral of the sum equals the sum of the integrals:

$$\phi_{Tot} = \phi_1 + \phi_2 \quad . \tag{2.71}$$

The potential at P (see Figure 2.10) for a single line charge with a reference level ϕ = 0 at R is given by

$$\phi = \frac{\rho_l}{2\pi\epsilon} \ln\frac{r}{R} \quad . \tag{2.72}$$

The individual potentials for a line 1 and a line 2 with a uniform dielectric will be

$$\phi_{Tot} = \frac{\rho_{l_1}}{2\pi\epsilon} \ln\frac{r_1}{R_1} + \frac{\rho_{l_2}}{2\pi\epsilon} \ln\frac{r_2}{R_2} \quad . \tag{2.73}$$

Now if $\rho_{l1} = -\rho_{l2} = \rho_l$, then the potential becomes

$$\phi_{Tot} = -\frac{\rho_l}{2\pi\epsilon} \left[\ln\frac{r_1}{R_1} - \ln\frac{r_2}{R_2}\right] = -\frac{\rho_l}{2\pi\epsilon} \ln\frac{r_1 R_2}{r_2 R_1} \quad , \tag{2.74}$$

and if the reference points are equal such that $R_1 = R_2$ where $\phi = 0$, the function becomes

$$\phi_{Tot} = -\frac{\rho_l}{2\pi\epsilon} \ln\frac{r_1}{r_2} = -\frac{\rho_l}{2\pi\epsilon} \ln\left[\frac{(x-d)^2 + y^2}{(x+d)^2 + y^2}\right]^{\frac{1}{2}} \quad . \tag{2.75}$$

Another way to write this is

$$\phi_{Tot} = \frac{\rho_l}{4\pi\epsilon} \ln\frac{(x+d)^2 + y^2}{(x-d)^2 + y^2} \quad . \tag{2.76}$$

The equipotentials are required next. The potential will be constant when the argument

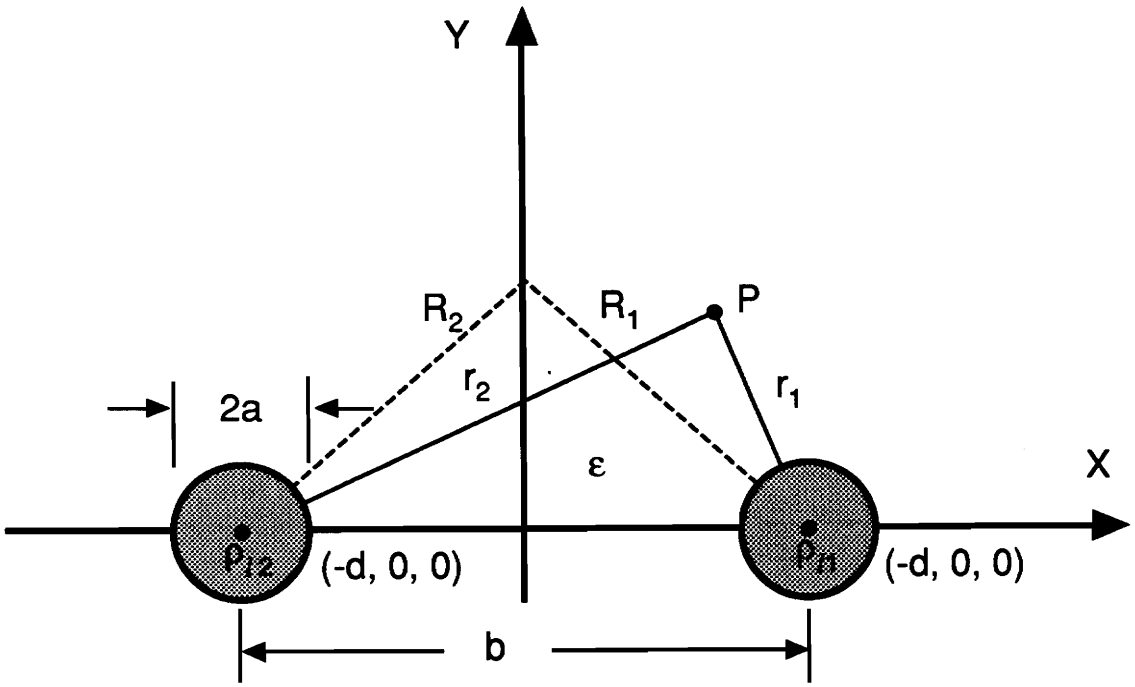

Figure 2.10 Two-Wire Potential Superposition

of the natural logarithm is constant:

$$\frac{(x+d)^2 + y^2}{(x-d)^2 + y^2} = K_1 \quad . \tag{2.77}$$

This can be rearranged to represent the equation for cylinders:

$$\left[x - d\frac{K_1+1}{K_1-1}\right]^2 + y^2 = \left[\frac{2d\sqrt{K_1}}{K_1-1}\right]^2 \quad . \tag{2.78}$$

From Equation 2.78, the axes for the cylinders are located at

$$x = d\frac{K_1+1}{K_1-1}, \quad y = 0, \tag{2.79}$$

and the radii are

$$\frac{2d\sqrt{K_1}}{K_1-1}, \quad for\ x > 0. \tag{2.80}$$

These parameters can now be represented by constants where

$$x_0 = d\frac{K_1+1}{K_1-1} \quad , \tag{2.81}$$

and

$$r_0 = \frac{2d\sqrt{K_1}}{K_1-1} \quad . \tag{2.82}$$

By solving for the parameters

$$\sqrt{K_1} = \frac{x_0 + \sqrt{x_0^2 - r_0^2}}{r_0} \quad , \tag{2.83}$$

and

$$d = \sqrt{x_0^2 - r_0^2} \quad , \tag{2.84}$$

the equation for an equipotential now becomes

$$V_0 = \frac{\rho_l}{4\pi\epsilon} \ln K_1 = \frac{\rho_l}{2\pi\epsilon} \ln\sqrt{K_1} \quad , \tag{2.85}$$

or

$$V_0 = \frac{\rho_l}{2\pi\epsilon} \ln \frac{x_0 + \sqrt{x_0^2 - r_0^2}}{r_0} \quad . \tag{2.86}$$

The voltage potential notation of V_0 has been substituted for the potential function ϕ_0 to simplify the transition to the electrical equations for capacitance. By noticing the symmetry of Figure 2.10, Equation 2.86 can be determined for $x < 0$. With a two-wire line, the potential difference is

$$V_0 - (-V_0) = 2V_0 \quad ; \tag{2.87}$$

so

$$2V_0 = \frac{\rho_l}{\pi\epsilon} \ln \frac{x_0 + \sqrt{x_0^2 - r_0^2}}{r_0} \quad . \tag{2.88}$$

The charge on the conductor is ρ_l. The capacitance becomes

$$C = Q/V_0 = \frac{\rho_l}{\frac{\rho_l}{\pi\epsilon}\ln\left[\left(x_0+\sqrt{x_0^2-r_0^2}\right)/r_0\right]} \quad , \tag{2.89}$$

and is simplified to

$$C = \frac{\pi\epsilon}{\ln\left[\left(x_0+\sqrt{x_0^2-r_0^2}\right)/r_0\right]} \quad (F/m) \quad . \tag{2.90}$$

By plugging in the specific values for x_0 and r_0, the solution becomes

$$C = \frac{\pi\epsilon}{\ln\left[\left(b/2+\sqrt{(b/2)^2-a^2}\right)/a\right]} \quad (F/m) \quad . \tag{2.91}$$

This solution can now be used to determine the impedance properties for the sensor cable in a uniform dielectric medium. The determination of the cable impedance for a two dielectric medium can be obtained from the same steps used in this derivation.

2.2.3 Capacitance for a Two-Wire Line in Two Dielectric Medium

The two dielectric case at a distance away from the conductors proves to be the same as the previous case. The two conducting wires are covered by an insulating dielectric ϵ_i and separated by a medium with a dielectric ϵ_s. The case for a single wire is superimposed to represent the case shown in Figure 2.11. The potentials for conductor 1 referenced from *a* are

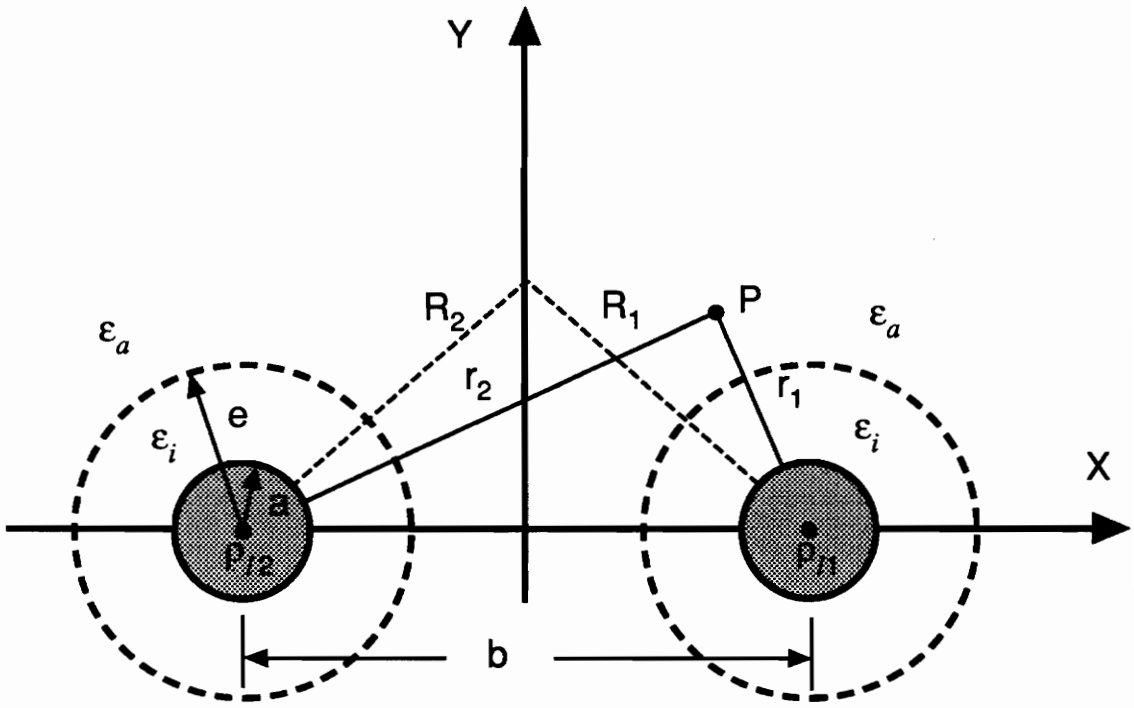

Figure 2.11 Two-Wire Line in a Two Dielectric Medium

$$\phi_{aR_1} = \frac{\rho_l}{2\pi\epsilon_a} \ln\frac{R_1}{a} + \frac{\rho_l}{2\pi\epsilon_i} \ln\frac{e}{a} \quad , \tag{2.92}$$

and

$$\phi_{ar_1} = \frac{\rho_l}{2\pi\epsilon_a} \ln\frac{r_1}{a} + \frac{\rho_l}{2\pi\epsilon_i} \ln\frac{e}{a} \quad . \tag{2.93}$$

The potentials for conductor 2 referenced from a are

$$\phi_{aR_2} = \frac{\rho_l}{2\pi\epsilon_a} \ln\frac{R_2}{a} + \frac{\rho_l}{2\pi\epsilon_i} \ln\frac{e}{a} \quad , \tag{2.94}$$

and

$$\phi_{ar_2} = \frac{\rho_l}{2\pi\epsilon_a} \ln\frac{r_2}{a} + \frac{\rho_l}{2\pi\epsilon_i} \ln\frac{e}{a} \quad . \tag{2.95}$$

By taking the difference between ϕ_{aR1} and ϕ_{ar1}, the potential between r_1 and the V = 0 reference point R_1 is found to be

$$\phi_{R_1r_1} = -\frac{\rho_l}{2\pi\epsilon_a} \ln\frac{r_1}{R_1} \quad . \tag{2.96}$$

The same approach can be used on conductor 2 to get

$$\phi_{R_2r_2} = -\frac{\rho_l}{2\pi\epsilon_a} \ln\frac{r_2}{R_2} \quad . \tag{2.97}$$

The solution now proceeds the same as for a single dielectric to give a superimposed potential of

$$\phi_{Tot} = -\frac{\rho_l}{2\pi\epsilon_a} \ln\frac{r_1}{r_2} = -\frac{\rho_l}{2\pi\epsilon_a} \ln\left[\frac{(x-d)^2 + y^2}{(x+d)^2 + y^2}\right]^{\frac{1}{2}} \quad . \tag{2.98}$$

The solution for capacitance is the same as for the uniform dielectric (see Equations 2.75-91) except the dielectric constant used is that of the surrounding medium, ϵ_a:

$$C = \frac{\pi\epsilon_a}{\ln\left[\left(b/2 + \sqrt{(b/2)^2 - a^2}\right)/a\right]} \quad (F/m) \quad . \tag{2.99}$$

This solution can be used to determine the impedance properties of widely spaced sensor cables.

Creativity requires the freedom to consider "unthinkable" alternatives, to doubt the worth of cherished practices.

- John W. Gardner

Chapter 3

Parametric Modeling

A health-monitoring system must be capable of operating within a variety of environments. The most effective system should have a design for which the parameter of interest has been optimized. To meet this criteria in the proposed TDR system, a set of parametric models has been used to design sensor cables for given case studies. The models are general enough to work for a variety of situations and material environments. This section discusses the development of the models and displays sample results for given cases.

For the application of TDR to damage sensing, specially designed sensing cables are important. The cables will be bonded on the structure surfaces or embedded within the structure. An example of a possible system is shown in Figure 3.1. A TDR system can then measure whatever has happened or is happening in the structure that affects the characteristic impedance of the sensing cables and interpret it as information on structural integrity. The cables need to be sensitive to the type of damage that is being monitored; therefore, three models have been used to explore their sensing abilities with TDR

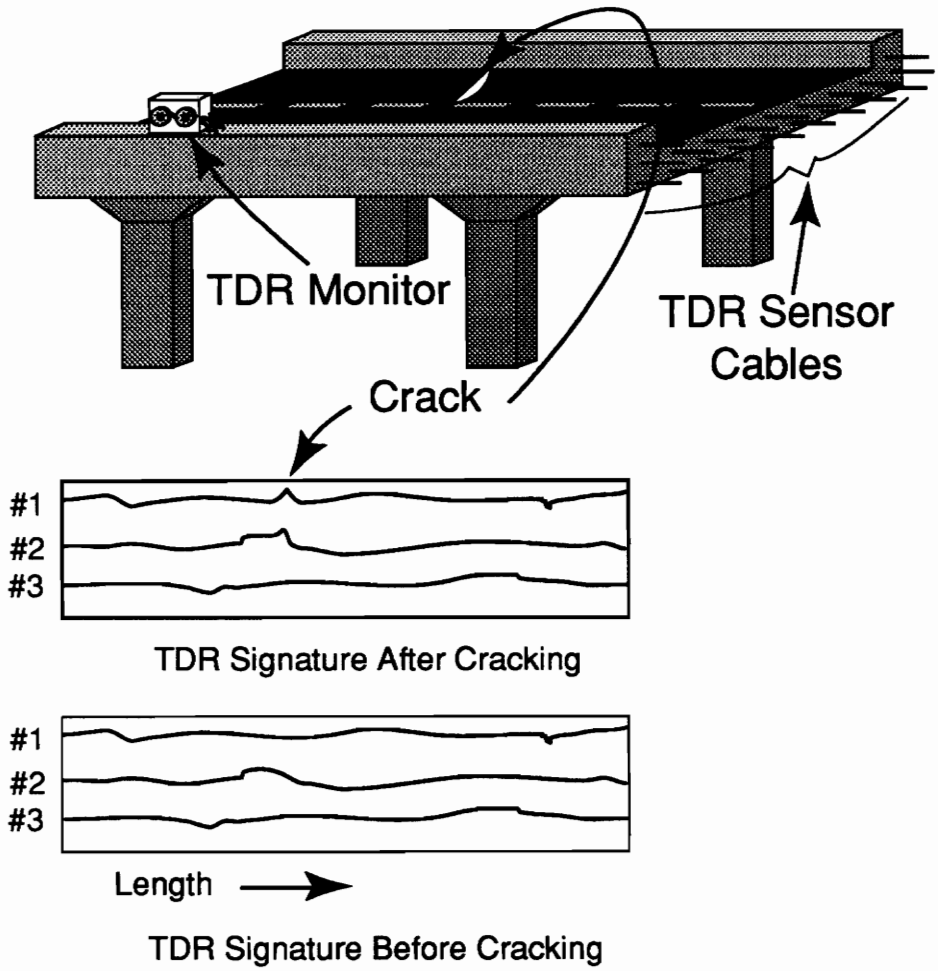

Figure 3.1 An example of a possible civil structure health-monitoring system (bridge with embedded TDR cables).

methods. One uses the equations developed from electric potential relationships for cable geometries. Another uses a finite element approach to model the capacitance response of coaxial cables. The third uses a Neumann (Silvester, 1968) inductance model to determine the TDR response for parallel cables.

3.1 Electric Potential-Based Models

The equations developed for a two-wire and a coaxial cable can be used for determining TDR response, but the primary mode of strain must be known. This mode may be determined from the shape of the TDR signal. Two MatLab (commercial matrix-based software for solving and plotting equations) programs, one for two-wire and one for coaxial cable, were used to computerize and therefore speed-up the calculations within the models. The main strain for the model case studies was considered to be axial. The TDR models were linked to an appropriate strain model to determine the TDR response for cables of varied parameters. Comparisons of the accumulated data were plotted for analysis of the reflection coefficients and the theoretical resolutions. These comparisons can now be used to determine the appropriate parameters for an axial strain sensitive cable (i.e., the cable with the greater reflection coefficient or impedance response for applied strain).

Expressions for the electrical properties of the cables can be derived from transverse electromagnetic (TEM) field theory. TEM fields are time-varying electromagnetic fields

that vary with position along all three coordinates in space, but which do not have a component of electric field or magnetic field in the specific direction (the longitudinal direction of the cable) in which electromagnetic signals and power are to be carried. Texts such as Elmore and Heald (1969), Neff (1981), and Sinnema (1979) explain the theory behind the expressions which relate cable parameters to the electric potential between conductors and electric potential to the electrical properties of impedance.

There are basically two types of sensing cables: parallel, and coaxial (see Figure 3.2 for geometric parameters). For the parallel two-wire cable shown in Figure 3.2a, there is no closed-form expression for its characteristic L, R, and C. If the isolation between the two wires is homogeneous and infinite, the capacitance from Equation 2.91 may be expressed as:

$$C = \frac{\pi \epsilon}{\ln\left(W/w+\sqrt{(W/w)^2-1}\right)} \quad , \tag{3.1}$$

where W=b and w=2a. By applying Equation 2.50 the inductance will be:

$$L = \frac{\mu}{\pi} \ln\left(W/w+\sqrt{(W/w)^2-1}\right) \quad , \tag{3.2}$$

where, for the two previous equations, ϵ is the dielectric constant and μ is the permittivity of the isolator between the conductors. The resistance is then based on the two conductor cross-sectional areas and the resistivity, ρ_c, of the materials used to make the conductors:

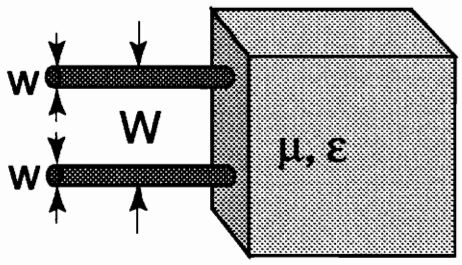

$$C = \frac{\pi\varepsilon}{\ln[W/w + \sqrt{(W/w)^2 - 1}]} \text{ F/m}$$

$$L = (\mu/\pi)\ln(2W/w) \text{ H/m}$$

$$R = \frac{2\rho_c}{\pi w^2}$$

ε = Permittivity

(a)

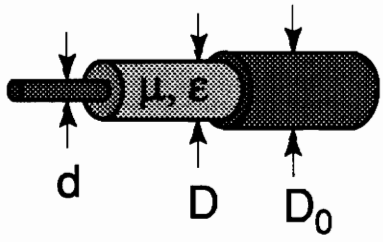

$$C = 2\pi\varepsilon/\ln(D/d) \text{ F/m}$$

$$L = (\mu/2\pi)\ln(D/d) \text{ H/m}$$

$$R = \frac{4\rho_c}{\pi(d^2 + D_0^2 - D^2)}$$

μ = Permeability

(b)

Figure 3.2 Parameters for the two types of sensing cables: (a) parallel two-wire, and (b) coaxial cable.

$$R = \frac{2\rho_c}{\pi w^2} \quad . \tag{3.3}$$

The dielectric constant ϵ is related to the relative dielectric constant by:

$$\epsilon_r = \epsilon/\epsilon_0 \quad , \tag{3.4}$$

where ϵ_0 is the dielectric constant of free space.

For the coaxial sensing cable as shown in Figure 3.2b, the characteristic capacitance can be expressed as:

$$C = \frac{2\pi\epsilon}{\ln(D/d)} \quad , \tag{3.5}$$

as previously noted in Equation 2.69. By applying Equation 2.50 the inductance would be

$$L = \frac{\mu}{2\pi}\ln(D/d) \quad . \tag{3.6}$$

The resistance

$$R = \frac{4\rho_c}{\pi(d^2 + D_0^2 - D^2)} \quad , \tag{3.7}$$

as with the two-wire cable, is calculated from the conductor cross-sectional areas and the resistivity.

Knowing the expression for the characteristic impedance of a sensing cable, the next step is the determination of the relationship between structural damage and its corresponding

variation in the characteristic line impedance.

Optimization of these cable sensitivities is achieved by relating the electrical properties of the cables to the dominating activation factor. The models used for these studies considered axial strain due to cracking to be the factor of interest. First, the model most appropriate for sensing axial strain is selected. One such model consists of a two-wire sensor with elastic conductors and plastic dielectric material. This model considers the relationship between axial strain and the size ratio to be:

$$W/w = W_0/w_0\left[\left(1 - 1/2\epsilon_l\right)/\left(1 - \nu_c\epsilon_l\right)\right] \quad , \tag{3.8}$$

where ν_c is the Poisson's ratio for the conductors and ϵ_l is axial strain. The line impedance is then:

$$Z_x = \sqrt{\frac{\mu}{\epsilon}}\,\frac{1}{\pi}\ln\left(W/w + \sqrt{(W/w)^2 - 1}\right) \quad . \tag{3.9}$$

A parametric study is used to determine the dominating parameters that provide the highest change in the line impedance due to local damages. The model plots, such as the sample runs in Figure 3.3, can then be used to determine which set of parameters meet the requirements for a particular sensing system. Table 3.1 and Table 3.2 give parameter values for typical conductors and dielectric isolators or insulation. Table 3.3 and Table 3.4 show the typical size ratios for commercially available coaxial and multi-wire cables. The selected parameter is matched to the appropriate materials or cables and then adjusted to provide the maximum sensitivity for the specified system.

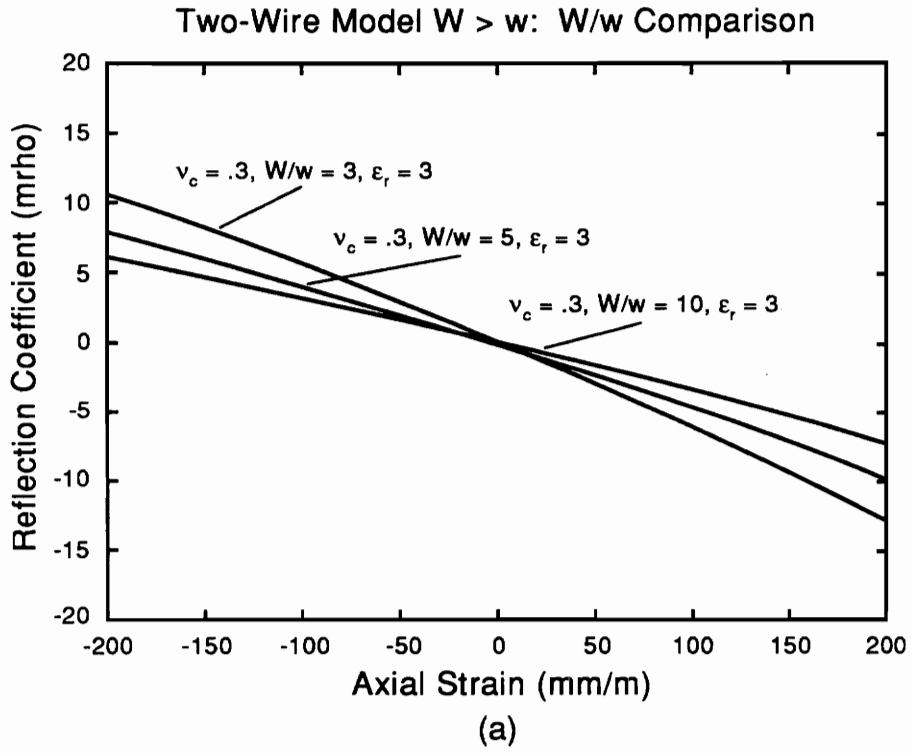

(a)

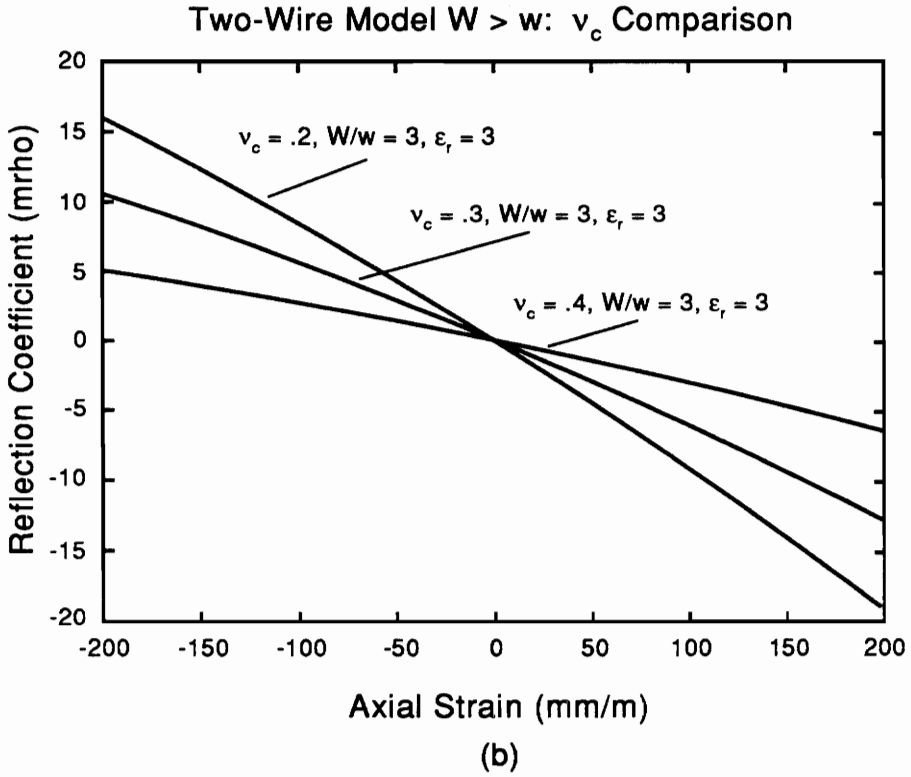

(b)

Figure 3.3 Plots for two-wire sensor model with elastic conductors and plastic dielectric. Altered parameters are: (a) size ratio W/w, and (b) Poisson's ratio ν_c.

Table 3.1 Insulation properties for data comparison (Parker, 1967).

Material	Relative Permittivity, ke	Conductivity, σ (Simiens/meter)	Tensile Modulus, E (GPa)
Air	1.0	-----	----
Teflon	2.1	10^{-16}	.400
Polyethylene (high density)	2.4	10^{-14}	.242
Polyethylene (low density)	2.4	10^{-14}	1.03
Rubber (butyl)	2.4	10^{-19}	.0069*
Silicone	2.6	10^{-13}	-----
Polyvinyl chloride	3.1	10^{-14}	4.13
Epoxy	4.0	10^{-12}	2.40
Nylon	4.7	10^{-13}	2.62
Glass (Soda lime)	7.2	$10^{-10.5}$	67.4

*@ 400% elongation

Table 3.2 Conductor properties for model comparison(Neff, 1981, and Juvinall,1983).

Material	Poisson's Ratio, vc	Resistivity, ρ_c (10^8 Ohm-meter)	Elastic Modulus, E (GPa)
Beryllium	.24	5.90	254
Iron (gray cast)	.26	9.71	196
Nickel	.30	6.84	206
Titanium	.30	47.8	116
Copper	.32	1.67	110
Graphite	.32	950	203
Aluminum	.33	2.66	68.8
Magnesium	.35	4.46	44.7
Silver	.37	1.59	75.6
Gold	.42	2.19	82.5

Table 3.3 Comparison data for typical coaxial cables (Sinnema, 1979).

Cable Type	Size Ratio, D/d	Velocity of Propagation, V_p/V_c
122/U	3.79	66.0%
141A/U	2.90	69.5%
174/U	3.77	66.0%
179B/U	6.30	69.5%
180B/U	10.2	69.5%

Table 3.4 Comparison data for typical two-wire cables (Micro-Measurements Division, 1982).

Cable Type	Size Ratio, W/w	Velocity of Propagation, V_p/V_c
Carol 2908	2.9	56.8%
Carol C1357	2.3	56.8%
326-DFV	2.5	56.8%
330-DFV	3.0	56.8%
330-FFE	3.0	69.5%

For example, a sensing system with a rise time of 45 pico seconds which requires a moderate spatial resolution (approximately 2 millimeters) and is composed of a two-wire sensor cable needs a relative dielectric constant of 2.8 (see Equation 1.13). From Table 3.1, a material similar to silicone would be chosen. The system does not need to sense more than a couple of strain sites, so a large reflection coefficient is desired from the cable. Figure 3.3 indicates that a small Poisson's ratio, ν_c, and a small shape ratio, W/w, will give the greater reflection coefficient change. Low resistance is also desired; therefore silver or copper would be selected from Table 3.2. The next step would be to locate a commercial cable that meets these specifications, or to create a new cable.

Future experiments will determine if the theoretical model predicts sensor sensitivities in a laboratory environment. Once the model is fine-tuned to adequate performance, a helpful design tool will be available for TDR sensors.

3.2 Finite Element Capacitance Model

Through refinement of an existing algorithm, a finite element model was developed to provide reflection coefficient information for a coaxial cable with capacitive change as the main mode of variation. The initial 2-D program was developed by Mia-Bin Su (1987) for his TDR research, but it only gave information on a single cross-section. The program was modified in this research to give the TDR response over the length of the

cable. This output can be analyzed to determine the best cable lengths and materials for a sensor cable.

The capacitive response of a coaxial cable was modelled by using a finite element program in BASIC. The model created a potential mesh for the dielectric material based on the outer diameters of the inner and outer conductors. The change in capacitance due to diameter changes and shape changes in a cable cross-section were then calculated over the length of a cable. Capacitance change due to shape change was considered to be the main source of impedance variation. All other impedance properties (resistance, inductance, and conductance) were either related to the capacitance or considered constant. The resolution of the cross-sections was also calculated by using rise time and dielectric constant information. The reflection coefficient was calculated over the length of the cable and output as a data file. The data was then plotted in the MatLab environment.

A sample of the model output is shown in Figure 3.4. Non-symmetrical geometry changes, such as shear strain, appear as sharp peaks or valleys on a reflection coefficient plot. Symmetrical geometry changes, such as axial strain, show a flat response on a reflection coefficient plot. The smoothness of a plot similar to Figure 3.4 is determined by the resolution equation used in the model and is typically given in the form of Equation 1.13. The effect of capacitive changes over the length of a cable can be grasped by a glance at the plotted output.

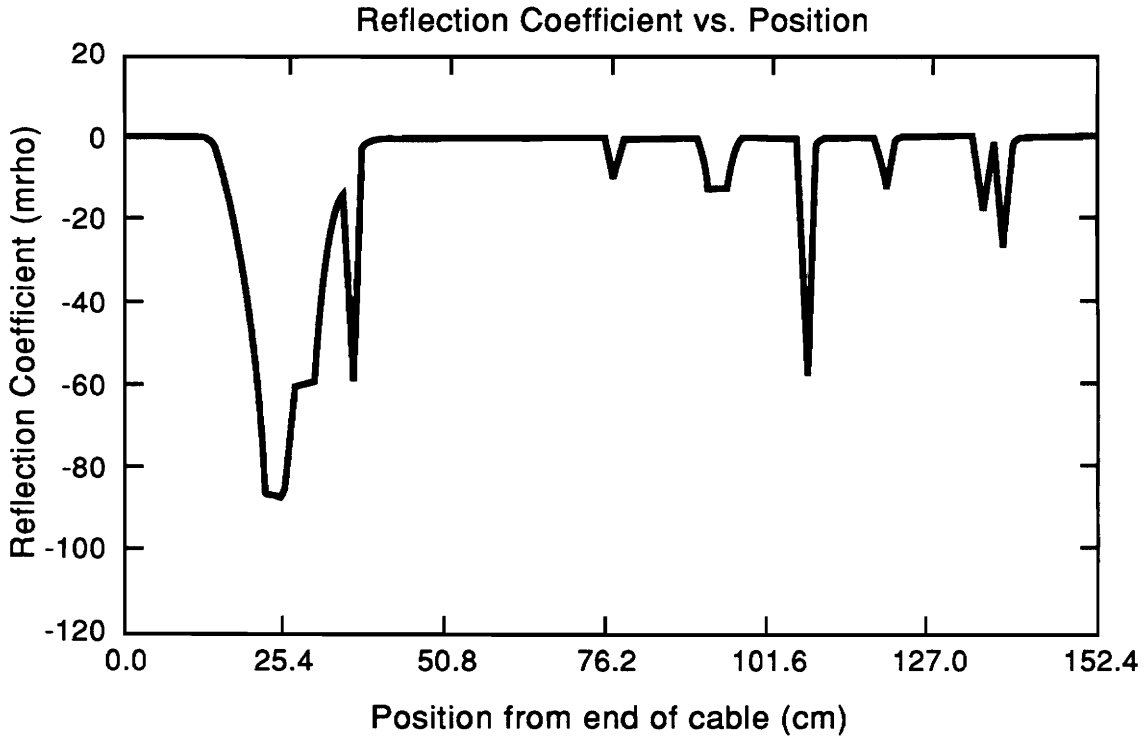

Figure 3.4 Sample TDR plot from capacitive finite element model.

The inputs for this model can be varied for different cable material properties and geometries to determine how they affect the TDR output. The model is very helpful for determining capacitive response over irregular cross-sections.

3.3 Neumann Inductance Model

A Neumann approach (Silvester, 1968) was also explored for a TDR model. Neumann developed an approximation for the inductance between two conducting bodies. This concept was applied to the cross-section of a two-wire cable.

A sequence of electromagnetic relationships were used to obtain the TDR response from the approximated inductance. For geometric changes in the cable, the conductance, G, and capacitance, C, were calculated from their relationship to the inductance, L. Resistance was calculated from the cross-sectional conductor (wire) areas. These electric properties were then used to calculate the impedance and subsequent TDR or reflection coefficient response.

A MatLab program was created to automate the numerical equations and to speed up the

calculations. The program was also capable of plotting the conductor contours. This method could have been adapted to 3-D responses; however, it only works for conductors in a uniform material. Comparisons could be developed between this model and the others to determine accuracy. The main benefit from this model was the ability to obtain TDR response for two irregular-shaped conductors or sensor wires.

There is no instrument so deceptive as the mind.

- St. John Ervine

Chapter 4

Resolution Experiments and Results

This chapter describes the reality of a TDR distributed sensing system. By theory it will work, but without data to support the theoretical work, the theory would be useless. The body of this chapter explains the experimental set-up used to get reinforcement data on spatial resolution, the process of taking data, and the results obtained from the experimental data.

4.1 Experimental Set-up

The experimental set-up is similar to the two-wire proof-of-concept experiment (see Figure 4.1). For the experiment described in Section 1.2, a qualitative value was achieved by pressing the operator's finger against the sensing cable. The material and equipment in these tests are the same; however, a known force was applied by hangers with various force application tips (see Figure 4.2). Knife edges, round contact surfaces, and flat contact surfaces were set on the cable to determine the shape sensing and/or pressure sensing capabilities as well as the resolution of a TDR sensing system. The

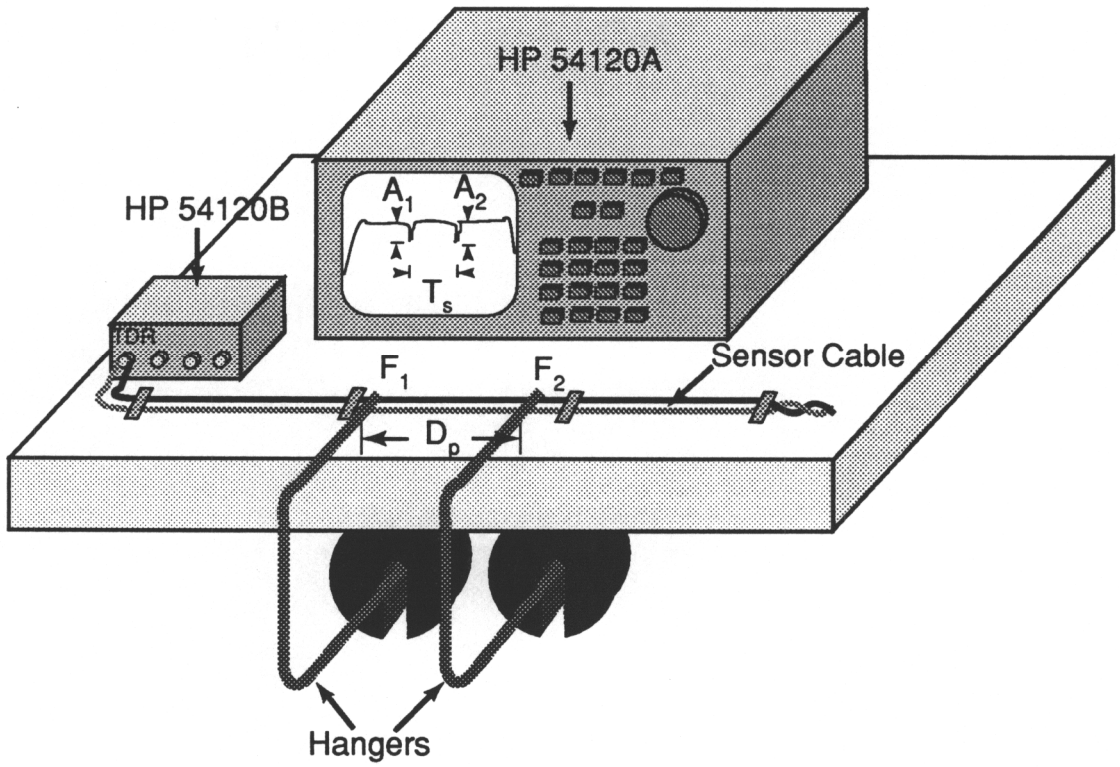

Figure 4.1 Experimental set-up.

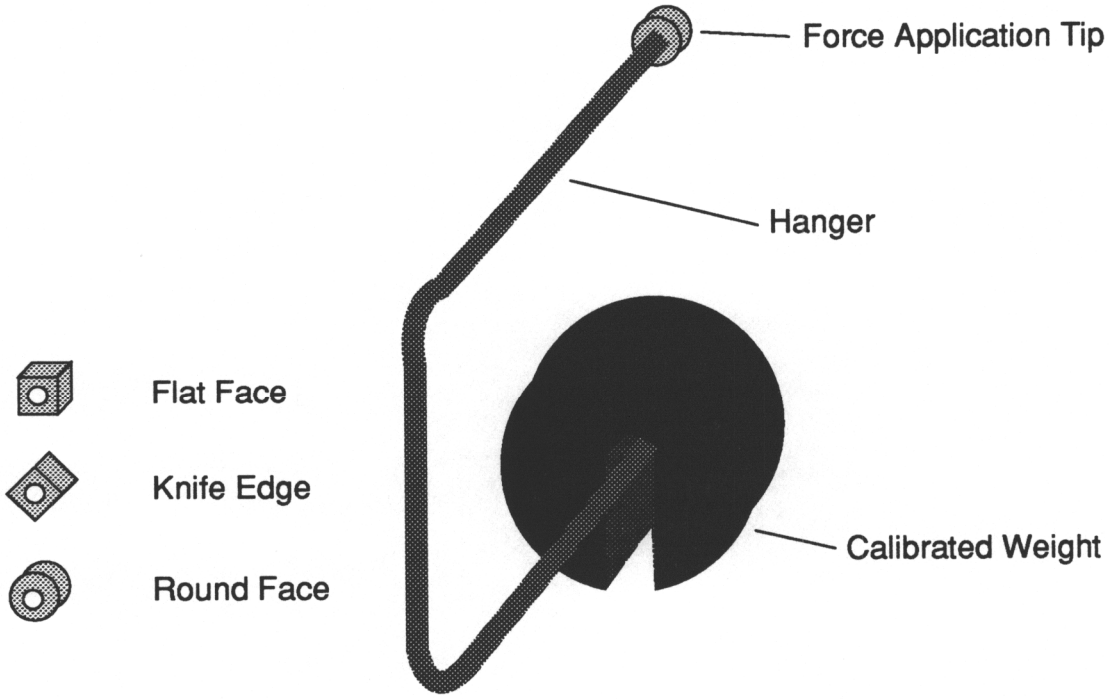

Figure 4.2 Hanger construction.

total applied force was determined by weighing the hanger/tip assembly and adding that to the calibrated weights which were hung from the hangers.

The HP 54120A and HP 54120B are the main electronics for the sensing system. These components are produced by Hewlett-Packard and are referred to, respectively, as the oscilloscope and TDR acquisition probe. The input impedance for the system is 50 ohms. The minimum and maximum input voltages are -0.2 and +0.2 volts. The small signal amplitude means that the signal will attenuate quickly. This limitation was also explored during the testing process.

The sensing cables were MM 330-DFV strain gage cable from the Micro-Measurements Division of Measurements Group, Inc. The cables consisted of three stranded tinned copper wires covered by a Vinyl (PVC) dielectric covering and placed together in a flat cable arrangement (Micro-Measurements Division, 1982). The test cables were stripped of one wire so that a two-wire cable was created for the experiment. The end of the cable was shorted to provide a recognizable end point on the oscilloscope.

The equipment was placed on a table top with the oscilloscope and TDR probe on one side and shorted cable end at the other side (refer to Figure 4.1). The cable was attached to the probe and then tacked to the table with cellophane tape at 30 centimeter (approximately 1 foot) intervals. The tacking was done to keep random cable movements from affecting the TDR readings. The oscilloscope was then adjusted until the tested

cable length was visible on the screen.

Data was recorded by taking pictures of the screen output and by writing down the force,voltage, and time for the individual force applications. Correlations between the applied force and the signal amplitude were derived from this data.

4.2 Experimental Process

The sensitivity and resolution of the TDR sensing system was derived through two testing processes. The two processes consisted of: 1) using incremental forces on a single hanger with a variety of force application tips to determine the force and shape (or pressure) sensitivity, and 2) using the most readable (greatest amplitude) application tip on multiple hangers with the same applied force to determine the minimum measurable distance between application points. The signal attenuation for increased cable lengths was obtained for both processes by performing the tests on six different cable lengths (30, 60, 120, 180, 240, 300 centimeters). The individual processes are described below.

4.2.1 Force and Shape Sensitivity

Each length of cable was attached to the TDR probe and then the oscilloscope was adjusted to give the most sensitive, yet distinguishable, picture over a 5 centimeter distance centered on the cable midpoint. A variety of forces (7.6, 25.4, 47.6, 69.8, and

89.1 N) were applied by the hanger and a reading was recorded for each application tip. A reading consisted of the amplitude and width of the signal measured on the scope. A picture was then taken of the screen output. The most distinguishable tip was then selected for the succeeding experiments.

4.2.2 Resolution

The oscilloscope was adjusted to show a 10 centimeter length starting from the cable midpoint and ending towards the shorted end of the cable. Two hangers with 25.4 N application forces were then placed at the ends of the examined cable length. The oscilloscope was examined to determine if the two application sites were distinguishable from one another. If they were, the hanger on the shorted end was moved towards the midpoint by incremental amounts (one centimeter and then one millimeter increments). The process was continued until the two application points appeared to be one point. A record was kept of the last distance between the hangers at which both application points were distinguishable. A picture was taken of the last two readings.

The ability of the system to sense multiple events was determined by setting the scope so that the whole cable was visible on the screen. Hangers with equal application forces and tips were then placed on the cable at recognizable (4-6 centimeter) intervals. The first hanger was placed at the cable midpoint and the hangers continued to be put on the cable until the last applied hanger was indistinguishable from the signal noise. The

number of applied hangers was then recorded.

4.3 Experimental Results and Discussion

The experimental results are given in the following sections. The data is expressed in various formats and discussed in the respective sections for force sensitivity and resolution.

4.3.1 Force and Shape Sensitivity

Plots of the TDR response are given in Figure 4.3. The responses shown were for a 120 centimeter cable with a 47.6 N application force. The variation in contact areas created differences in the TDR response. Wider contact surfaces gave a wider response with greater amplitude. The amplitude increased with the application of more force; however, at forces above 69.8 N the narrower application tips gave a sharply increasing signal amplitude. This was caused by the intense contact pressure which flattened and began to cut through the cable.

The most readable signal was obtained from the 1.27 centimeter Flat Face. Force and TDR response were recorded for the various cable lengths and plotted for comparison in Figure 4.4. The noise in the signals complicated the amplitude readings, but a general trend toward signal attenuation is indicated for the longer cables. The plots also showed

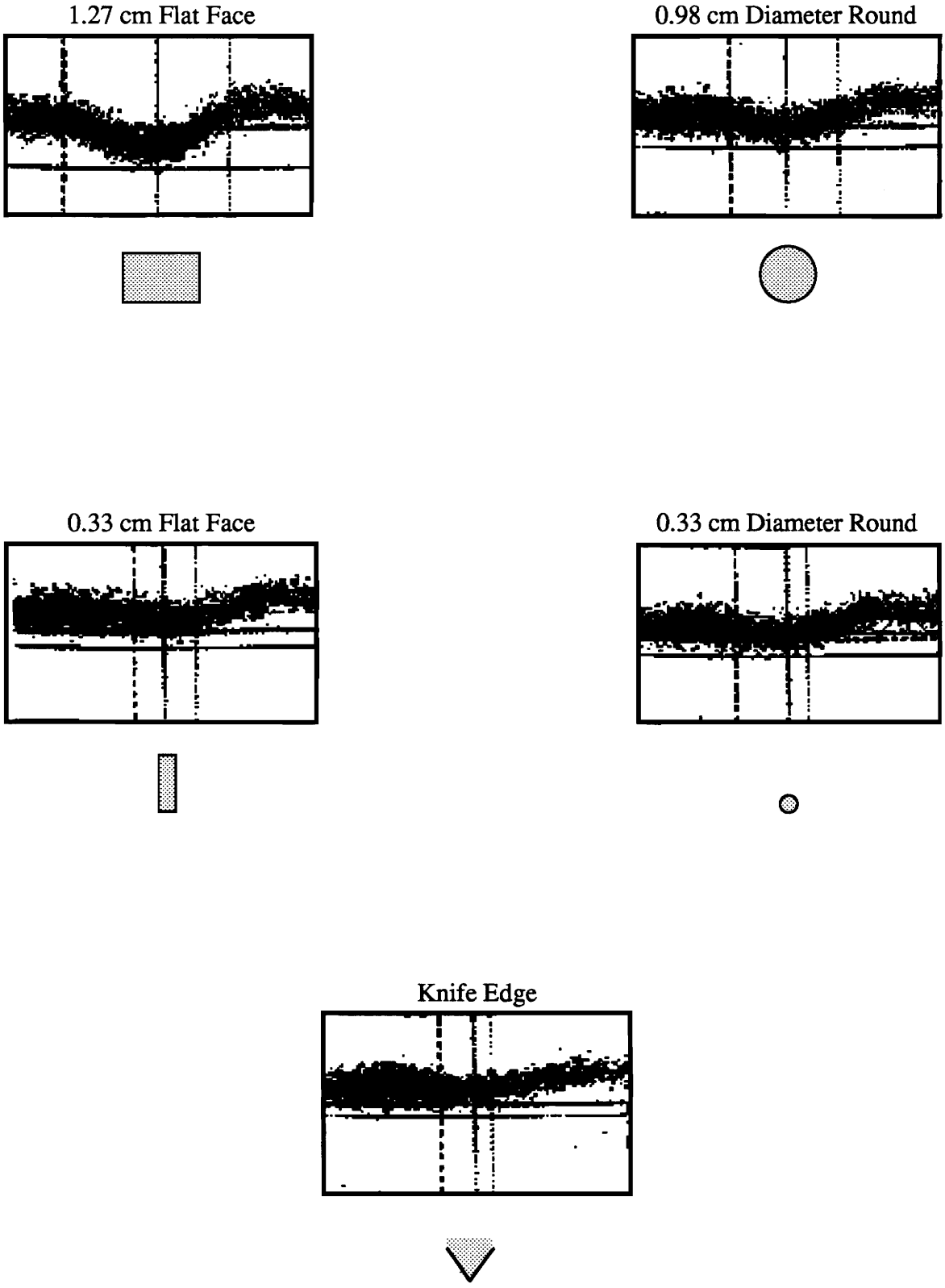

Figure 4.3 Sample shape plots.

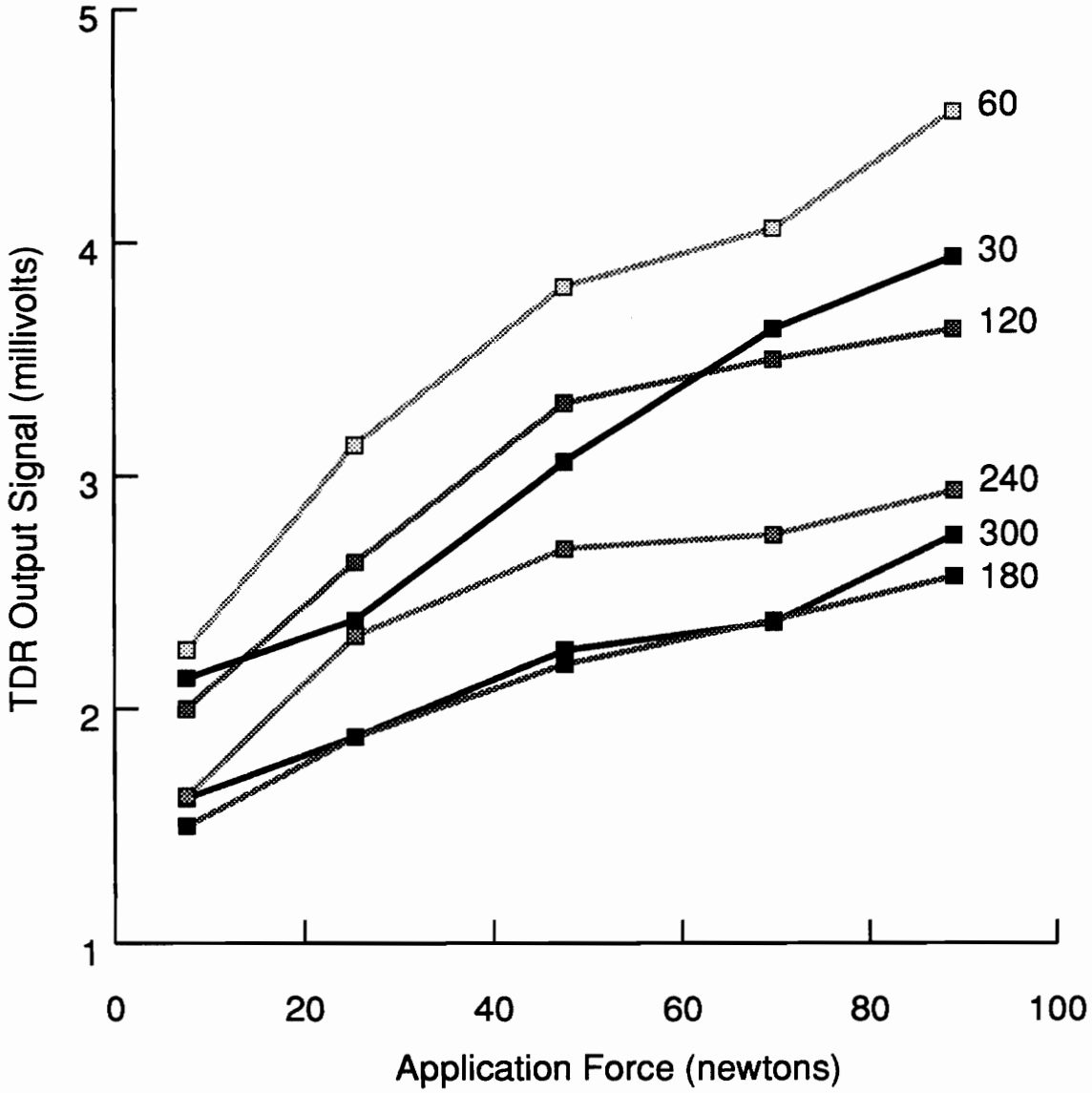

Figure 4.4 Force to TDR comparison plot as a function of cable length.

a near linear relationship between the force and the TDR signal. More test runs with the various lengths of cable would allow data averaging and, subsequently, the mean values would have confidence limits that indicate the uncertainty of the data. This is suggested for future correlation between the TDR signal and applied forces.

4.3.2 Resolution

The larger Flat Face was chosen for the resolution experiments. The predicted resolution (1.9 millimeters) from Equation 1.13 is shown in Figure 4.5 as a function of the system rise time. This is given as the distance between two application points at which the TDR signal appears to come from one application point. Hewlett-Packard (1987) suggests the practical distance between observable points is actually twice that amount, or 3.8 millimeters.

The resolution readings (distance between points) were taken during the transformation between the single and double point sites (see Figure 4.6). The results were about a factor of ten greater than predicted (see Figure 4.7). The readings varied from 2-3 centimeters which gives a predicted resolution of 4-6 centimeters. The difference in results may be due to the cable impedance.

The HP 54120 is designed for use with cable of 50 ohms, but the MM 330-DFV cables have a nominal impedance of approximately 122 ohms. No correction factor is given in

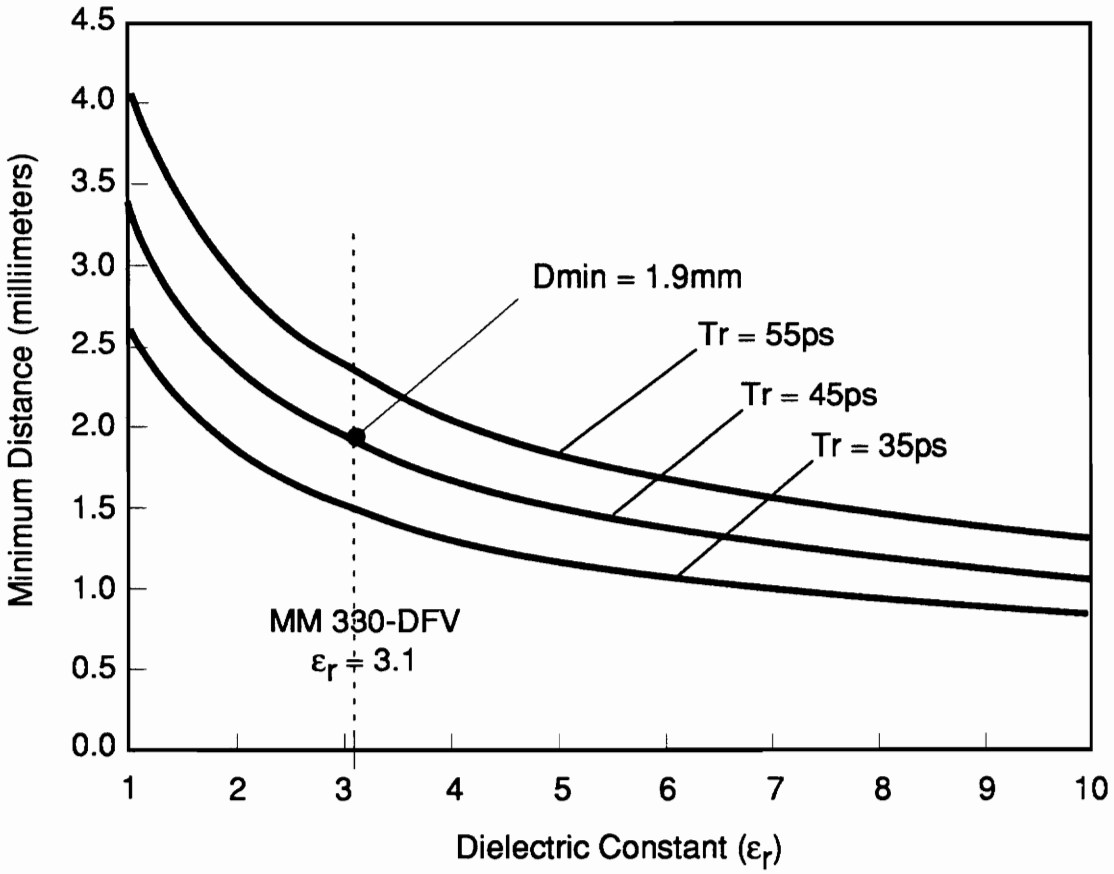

Figure 4.5 Predicted minimum resolution distance as a function of T_r.

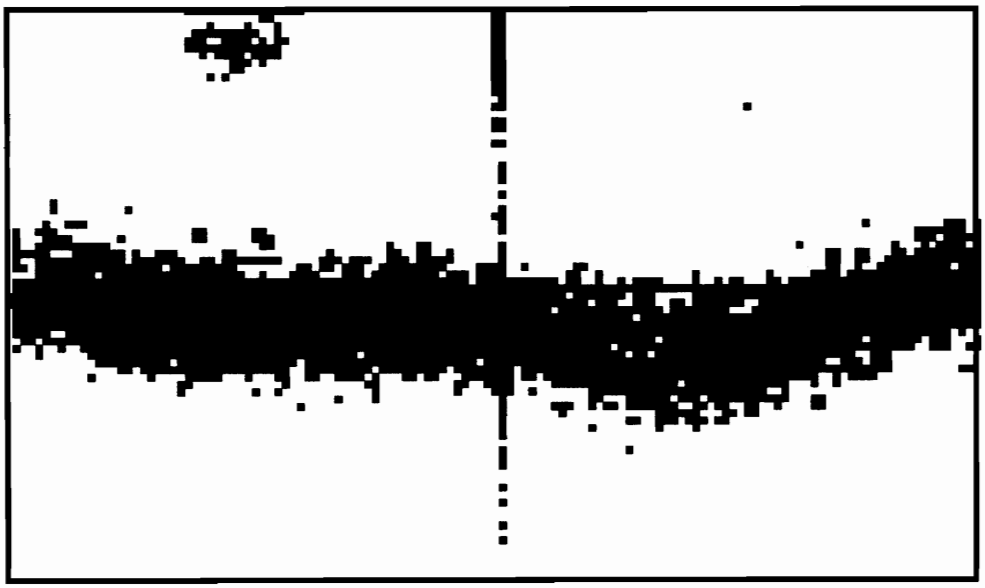

(a)

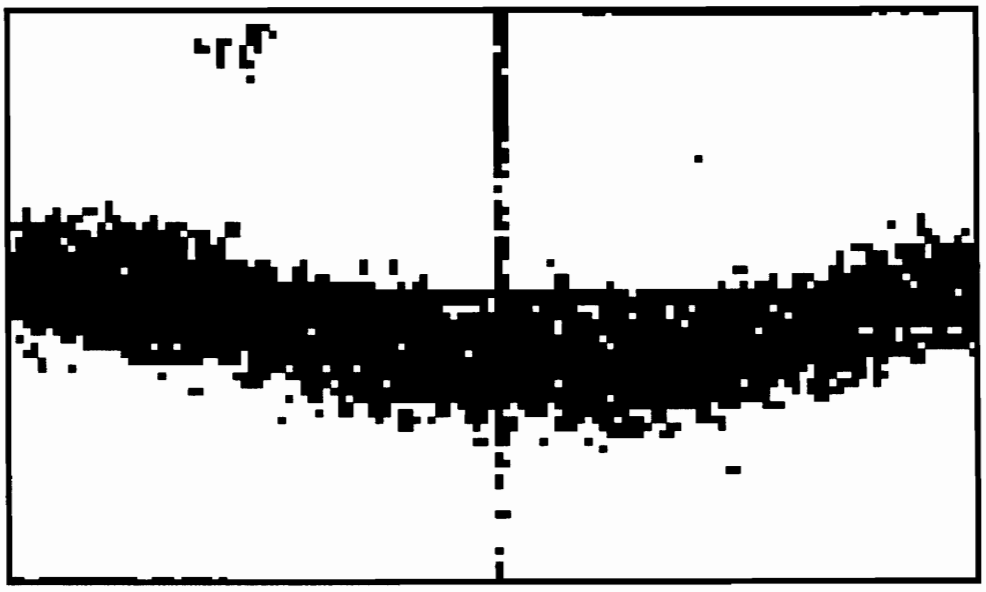

(b)

Figure 4.6 Resolution change between two points at (a) 3 centimeters and (b) 2 centimeters.

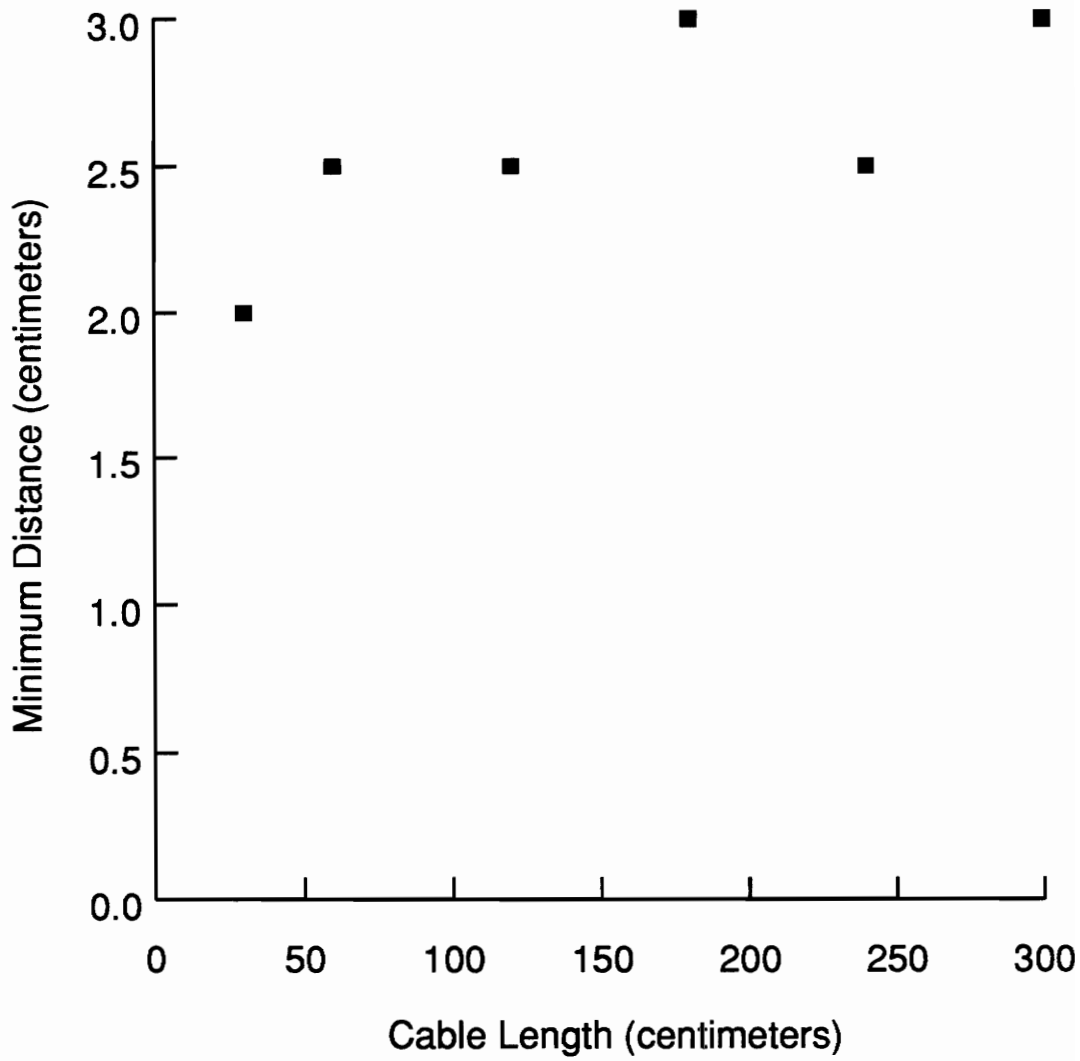

Figure 4.7 Actual minimum resolution.

the manuals. More research into this area may give a less simplified solution for resolution that includes an impedance component.

The main limitation in the number of sensed events was the practical resolution for the cables. The cable length could have been divided by the practical resolution to determine the number of sensed events rather than counting them (see Figure 4.8). The main limitation of the system is then the resolution between two points, because a single event could be sensed anywhere along the cable. Future work should then be directed towards reducing the minimum sensed distance between two application sites.

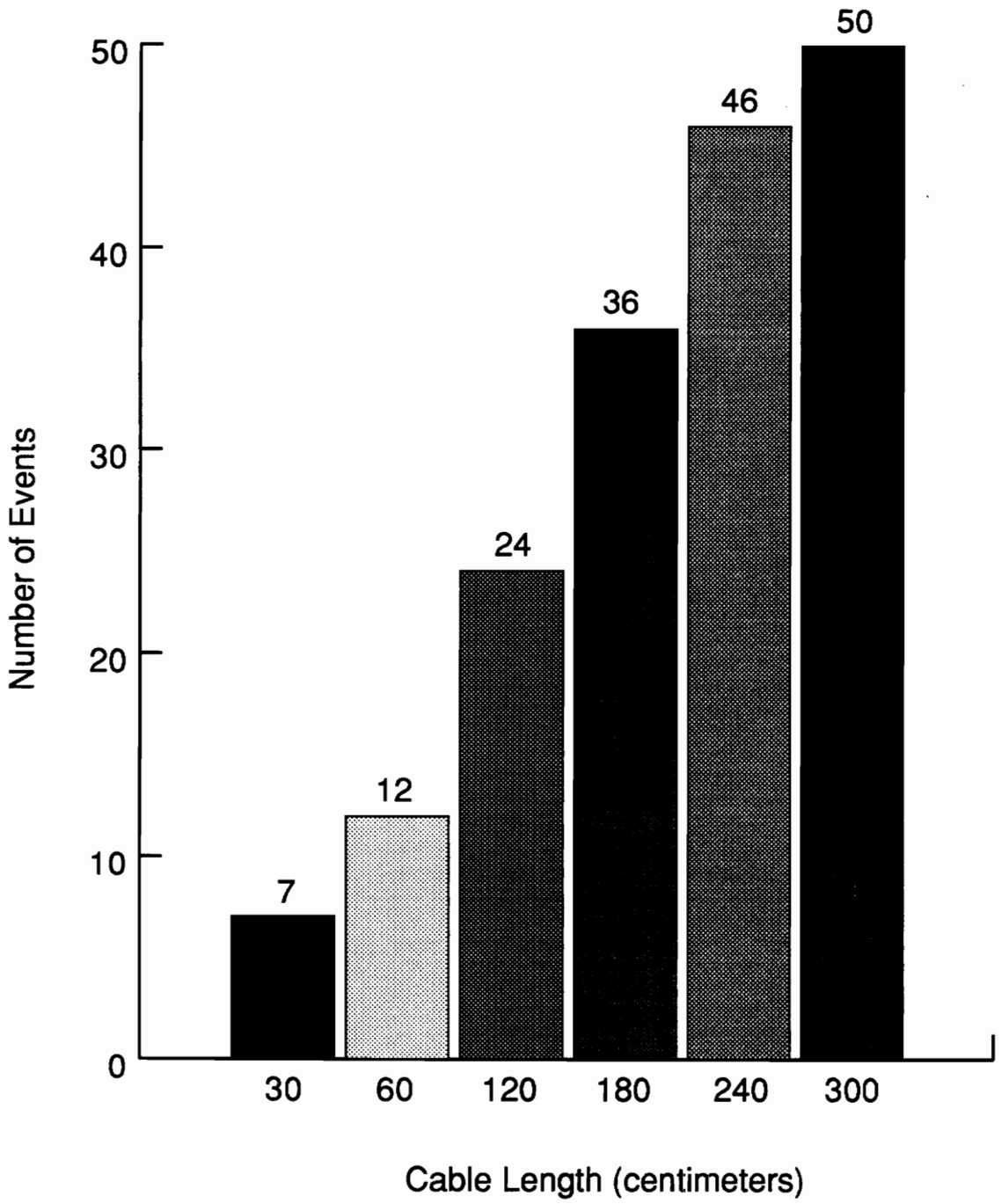

Figure 4.8 Plot of cable length versus number of event sites.

"I think I understand you humans at last," Charlie told them...

"One of your ancient writers, a historian named Heredontus, tells of a thief who was to be executed. As he was taken away he made a bargain with the king: in one year he would teach the king's favorite horse to sing hymns."

"The other prisoners watched the thief singing to the horse and laughed. 'You will not succeed,' they told him. 'No one can.' To which the thief replied, 'I have a year, and who knows what might happen in that time. The king might die. The horse might die. I might die. And perhaps the horse will learn to sing.'"

- The Motie alien Charlie explaining the human drive to look for solutions even in impossible situations. Taken from "The Mote in Gods Eye" by Larry Niven and Jerry Pournelle.

Chapter 5

Conclusions and Recommendations

The main purpose of this thesis was to propose an application for a time-proven method of sensing and show that it could be adapted to a new environment, intelligent sensing. The feasibility and limitations of this technique were explored and perhaps advanced beyond the realm of theory. The results of this work are summed-up in the conclusions section and recommendations for further research are proposed in the final section.

5.1 Conclusions

The goals of this project were met. The idea of using TDR techniques for a structural sensing device has been advanced to working models. The detail and responsiveness of the models must be refined for more accuracy, but the general characteristics of the models correspond to the experimental results. The elastic models or equations must also be refined to more accurately represent the relationship between the embedded structure, the sensing cable, and the TDR equipment.

This work has contributed to the development of a damage detection system in two areas. First, models to design cables for specific environments have been created and used to select optimum cable parameters. Second, preliminary experiments determined the real output of a designed system and the improvements needed in the model.

Various demonstration experiments have shown that TDR can be an effective method for damage detection. These and other experiments show that this system is well suited for harsh environments with large strains or forces. The resolution experiments demonstrated the sensitivity of a TDR sensing system was dependent on the minimum distance between multiple application sites. The large strain and selective sensitivity of the system indicate the technique would work well in a civil structure environment.

5.2 Recommendations

The information gained in this project was a large step towards the development of an operating TDR distributed sensing system; however, a lot of work must still be done. Suggestions for areas of improvement include:

The experiments and the theoretical models should be examined to determine where further improvements can be made to get closer agreement between the two. Perhaps by refining the TEM models of sensor cables greater resolution and event sensing may be possible in the damage detection systems.

TDR equipment should be considered a high priority for future development. The equipment should be selected from more recent models with greater capabilities. Such items as variable input impedance and larger pulse generation would greatly enhance the responsiveness.

Civil structures within corrosive or rugged environments should be targeted for these systems due to the toughness of the two-wire or coaxial cables. Selective placement such as in a bridge piling could provide warning before failure occurs.

Interfacing the TDR system with a computer would simplify data acquisition and plotting. Averaging schemes could then be implemented for cleaner signals.

The sensing system and the design models should be run on a variety of sensor cables to show the compatibility of the TDR techniques within different structures. Multiple tests on the previously tested MM 330-DFV cables mustbe done to add statistical stability to the results presented in Chapter 4.

References

Amato, I., (1992), "Animating the Material World," *Science*, Vol. 255, pp. 284-286.

Castro, J., (1989), "The Benefits of Being Prepared: Emergency Planning Paid Off but did not Prevent Two Disastrous Collapses," *Time*, Vol. 134, October 30, p. 42.

Chong, K. P., Scalzi, J. B. and Dillon, O. W., (1990), "Overview of Nondestructive Evaluation Projects and Initiative at NSF," *Journal of Intelligent Material Systems and Structures*, Vol. 1, No. 4, October 1990, pp. 422-431.

Clemeña, G. C., (1987), *Determining Water Content of Fresh Concrete by Microwave Reflection or Transmission Measurement*, Final Report to Virginia Transportation Research Council, Charlottesville, Virginia, VTRC 88-R3, August 1987.

Coleman, C., (1990a), "The Distributed Sensor," U. S. Patent Proposal for the Smart Materials Laboratory, Virginia Polytechnic Institute and State University, Blacksburg, Virginia.

Coleman, C., (1990b), "Common Forms of Gaging Concrete," Smart Materials Laboratory Memo, Virginia Polytechnic Institute and State University, Blacksburg, Virginia.

Crawley, E. F. and de Luis, J., (1987), "Use of Piezoelectric Actuators as Elements of Intelligent Structures," *AIAA Journal*, Vol. 25, No. 10.

Dick, R. D., and Parrish, R. L., (1986), "Instrumentation Techniques for Monitoring Shock and Detonation Waves," *Experimental Techniques*, August, pp. 26-31.

Dorenbos, P., and den Hartog, H. W., (1988), "A Time Domain Reflectometry Set-Up for Measuring Ionic Conductivity and Permittivity at High Temperatures," *Journal of Physics E: Scientific Instruments*, Vol. 21, pp. 171-178.

Dowding, C. H., O'Connor, K. M., and Su, M. B., (1989), "Measurement of Rock Mass Deformation with Grouted Coaxial Antenna Cables," *Rock Mechanics and Rock Engineering*, Vol. 22, pp. 1-23.

Dry, D., (1992), "Passive Smart Materials for Sensing and Actuation," *Proceedings of the Conference on Recent Advances in Adaptive and Sensory Materials and Their Applications*, Blacksburg, VA, April 27-29, pp. 207-223.

Elmore, W. C., and Heald, M. A., (1969), *Physics of Waves*, McGraw-Hill, Inc., New York.

Gerardi, T. G., (1990), "Health Monitoring Aircraft," *Journal of Intelligent Material Systems and Structures*, Vol. 1, No. 3, July 1990, pp. 375-385.

Hewlett-Packard, (1987), "TDR Fundamentals," *HP54120T User Reference Manual*, Appendix C, pp. C1-C37.

Ikegami, R., Wilson, D. G., Anderson, J. R., and Julien, G. J., (1990), "Active Vibration Control Using NiTiNOL and Piezoelectric Ceramics,"*Journal of Intelligent Material Systems and Structures*, Vol. 1, No. 2, April 1990, pp. 189-206.

Jackson, B. C., (1984), *Optical Time Domain Reflectometry as a Nondestructive Evaluation Technique for Composite Materials*, Masters Thesis, Virginia Polytechnic Institute and State University, Blacksburg, Virginia.

Jones, R., (1962), *Non-Destructive Testing of Concrete*, Cambridge at the University Press, Cambridge.

Jones, R. M., (1975), *Mechanics of Composite Materials*, Hemisphere Publishing Corporation, New York, p. 1.

Juvinall, R. C., (1983), *Fundamentals of Machine Component Design*, John Wiley and Sons, Inc., New York, p. 619.

Measures, R. M., (1989), "Smart Structures with Nerves of Glass," *Journal of Progress in Aerospace Science*, Vol. 26, pp. 289-351.

Micro-Measurements Division, (1982), *M-Line Strain Gage Accessories*, Catalog A-110-3, Measurements Group, Inc., Raleigh, North Carolina.

Miller, E. K., Editor, (1986), *Time Domain Measurements in Electromagnetics*, Von Nostrand Reingold Co., New York.

Moffitt, L. R., (1964), "Time Domain Reflectometry - Theory and Applications," *Engineering Design News*, November, pp. 38-44.

Neff, H. P., (1981), *Basic Electromagnetic Fields*, Harper & Row, Publishers, Inc., New York.

O'Lone, R. G., (1988), "Aloha Airlines," *Aviation Week and Space Technology*, Vol. 128, pp. 16-18.

Ouyang, C., Landis, E., and Shala, S. P., (1991), "Damage Assessment in Concrete Using Quantitative Acoustic Emission," *Journal of Engineering Mechanics*, Vol. 117, No. 11, November 1991, pp. 2681-2698.

Panek, L. A., and Tesh, W. J., (1981), *Monitoring Ground Movements Near Caving Slopes - Methods and Measurements*, RI 8585, U. S. Bureau of Mines, Denver, Colorado, p. 108.

Parker, E. R., (1967), *Materials Data for Engineers and Scientists*, McGraw-Hill Book Company, New York, pp. 318-352.

Rogers, C. A., Li, S., and Liang, C., (1991), "Active Damage Control of Hybrid Material Systems Using Induced Strain Actuators," *Proceedings of the 32nd Structures, Structural Dynamics and Materials Conference*, Baltimore, MD, April 1991, #AIAA 91-1145, pp. 1190-1203.

"S. S. Schenectady," (1943), *Ship Structures Committee*, U. S. Government, December 16, 1943.

Silvester, P., (1968), *Modern Electromagnetic Fields*, Prentice-Hall, Inc., Englewood Cliffs, NJ.

Sinnema, W., (1979), *Electronic Transmission Technology*, Prentice-Hall, Inc., Englewood Cliffs, NJ.

Strickland, J. A., (1970), *Time-Domain Reflectometry Measurements*, Tektronics, Inc., Beaverton, OR.

Su, M. B., (1987), *Quantification of Cable Deformation with Time Domain Reflectometry Techniques*, Doctoral Dissertation, Northwestern University, Evanston, IL.

Topp, G. C., Davis, J. L., and Annan, A. P., (1980), "Electromagnetic Determination of Soil Water Content: Measurements in Coaxial Transmission Lines," *Water Resources Research*, Vol. 16, No. 3, pp. 574-582.

Vita

On June 9, 1967, Jeffrey Allen Stastny was born in Klamath Falls, Oregon. He was raised in Malin, Oregon and graduated from Lost River High School on June 9, 1985. He continued his education at Oregon State University where he pursued an undergraduate degree in Mechanical Engineering. He recieved his bachelor's degree from the Mechanical Engineering Department on June 10, 1989. He then attended Virginia Tech to begin research work towards a Master of Science degree in the Mechanical Engineering Department. He completed this degree in October of 1992. He plans to begin an engineering career in the Pacific Northwest.